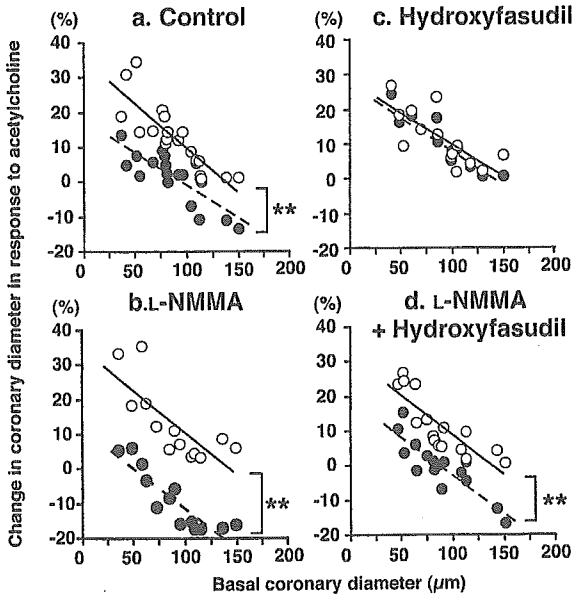

Figure 5. Coronary microvascular responses to acetylcholine before and after coronary ischemia/reperfusion (I/R) injury in dogs in vivo. Under control conditions, I/R significantly impaired coronary vasodilator response to acetylcholine **(a)**, whereas hydroxyfasudil completely preserved the responses in the absence **(c)** or presence of L-NMMA **(d)** compared with that in the presence of L-NMMA alone **(b)**. Number of vessels per animals used was 19/7 under control conditions (before I/R: $y = -0.3x + 35.9$, $r = 0.85$; after I/R: $y = -0.2x + 18.1$, $r = 0.80$), 13/4 for L-NMMA alone (before I/R: $y = -0.2x + 35.1$, $r = 0.76$; after I/R: $y = -0.2x + 12.2$, $r = 0.88$), 14/7 for hydroxyfasudil (before I/R: $y = -0.2x + 27.9$, $r = 0.73$; after I/R: $y = -0.2x + 27.4$, $r = 0.80$), and 16/7 for hydroxyfasudil plus L-NMMA (before I/R: $y = -0.2x + 31.8$, $r = 0.83$; after I/R: $y = -0.2x + 19.2$, $r = 0.86$). **$p < 0.01$. **Open circles** = before I/R; **solid circles** = after I/R.

variables at baseline did not significantly change after I/R compared with those before I/R (Table 1).

Effects of Rho-kinase inhibition on serotonin-induced coronary responses. Intracoronary administration of serotonin caused coronary vasoconstriction of small arteries and vasodilation of arterioles under control conditions (Figs. 3a and 3b, both $p < 0.01$ vs. basal coronary diameter). Intracoronary administration of L-NMMA enhanced the serotonin-induced vasoconstriction and abolished the serotonin-induced vasodilation of arterioles (Fig. 3b, $p < 0.01$ vs. serotonin, S). By contrast, hydroxyfasudil reversed the serotonin-induced vasoconstriction of small arteries to vasodilation while it further enhanced the serotonin-induced vasodilation of arterioles (Figs. 3a and 3b, both $p < 0.01$). The vasodilator effect of hydroxyfasudil on the coronary response to serotonin was significantly attenuated by L-NMMA in both-sized arteries (Figs. 3a and 3b, both $p < 0.01$). As a result, serotonin-induced increase in CBF (Fig. 3c) was significantly inhibited by L-NMMA ($p < 0.05$) and enhanced by hydroxyfasudil ($p < 0.05$), the effect of which was significantly attenuated by L-NMMA ($p < 0.01$).

Endothelium-dependent coronary vasodilation before and after I/R. Under control conditions (before I/R), intracoronary administration of acetylcholine caused a significant coronary vasodilation to a greater extent in arterioles than in small arteries (Figs. 4a, 4b, and 5a, $p < 0.01$). Coronary I/R significantly impaired the coronary vasodilation to acetylcholine in both sized arteries (both $p < 0.01$) and L-NMMA further reduced the vasodilation (Figs. 4a, 4b, and 5b both $p < 0.01$), whereas hydroxyfasudil completely preserved (small artery $p < 0.05$, arteriole $p < 0.01$) the acetylcholine-induced coronary vasodilator response after I/R (Figs. 4a and 4b). The vasoconstriction by L-NMMA was significantly attenuated by hydroxyfasudil in both sized arteries (both $p < 0.05$) with decrement of CBF (Figs. 4a to 4c). When the coronary vasodilator response to acetylcholine was expressed as a function of basal coronary diameter, hydroxyfasudil preserved the response after I/R injury at all sized coronary arteries either in the absence

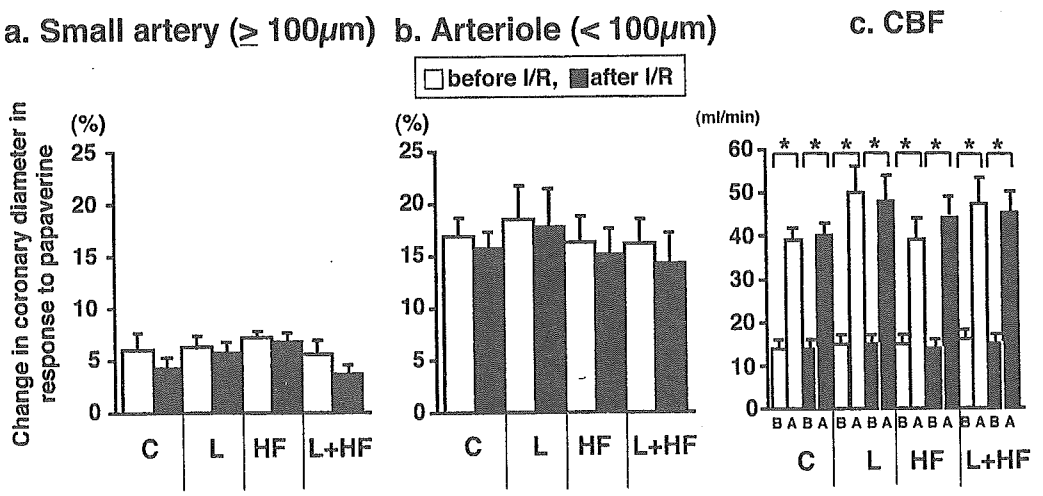

Figure 6. Endothelium-independent coronary vasodilation before and after coronary I/R injury in dogs in vivo. Coronary vasodilator response to papaverine was comparable under all conditions in both small arteries and arterioles. Number of vessels per animals used was 7/6 for control (mean diameter 120 ± 7 μm), 5/4 for L-NMMA (123 ± 8 μm), 6/4 for hydroxyfasudil (118 ± 8 μm), and 5/4 for hydroxyfasudil plus L-NMMA (125 ± 9 μm) in small arteries; and 12/6 for control (70 ± 6 μm), 8/4 for L-NMMA (69 ± 7 μm), 8/5 for hydroxyfasudil (68 ± 7 μm), and 11/6 for hydroxyfasudil plus L-NMMA (71 ± 5 μm) in arterioles. C = control; L = L-NMMA; HF = hydroxyfasudil. I/R = ischemia/reperfusion. B = before papaverine; A = after papaverine.

JACC Vol. 45, No. 4, 2005
February 15, 2005:599–607

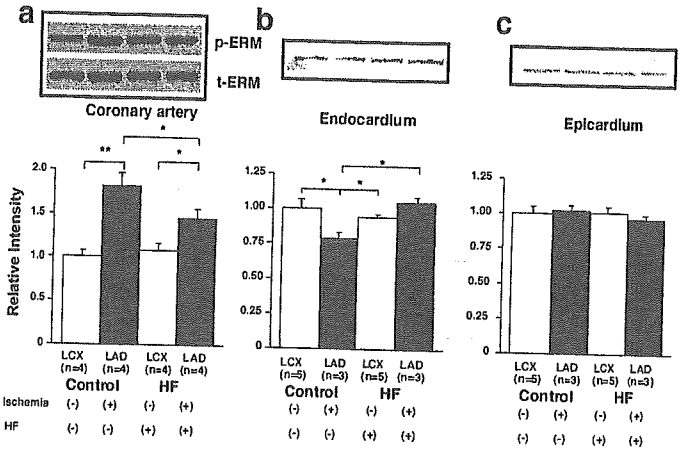

Figure 7. Western blotting showing the effects of hydroxyfasudil (HF) on Rho-kinase activity and on eNOS protein expression in the myocardium of LAD and LCX. **(a)** Rho-kinase activity in coronary artery; **(b)** expression of eNOS protein in endocardium; **(c)** expression of eNOS protein in epicardium. Rho-kinase activity was determined by the degree of ezrin-radixin-moesin phosphorylation (p-ERM/t-ERM). Rho-kinase activation in the ischemic LAD was completely inhibited by cotreatment with hydroxyfasudil. Expression of eNOS protein in the ischemic endocardium of LAD area was significantly decreased compared with the non-ischemic endocardium of LCX area, which was again improved by hydroxyfasudil. $^{*}p < 0.05$, $^{**}p < 0.01$.

(Figs. 4a, 4b, and 5c, df 2, 25, $p < 0.01$) or presence (Figs. 4a, 4b, and 5d, df 2, 24, $p < 0.01$) of L-NMMA compared with that in the presence of L-NMMA alone (Figs. 4a, 4b, and 5b).

Endothelium-independent coronary vasodilation. Coronary vasodilator response to papaverine was comparable under all conditions in both small arteries and arterioles (Figs. 6a and 6b). Similarly, the increase in CBF to papaverine (Fig. 6c) was also comparable under all conditions in both-sized arteries. Those coronary vasodilator responses were resistant to the blockade of NO synthesis with L-NMMA (Figs. 6a and 6b).

Activation of Rho-kinase by ischemia-reperfusion causes down-regulation of eNOS protein expression. Rho-kinase activity after a 90-min period of ischemia was significantly greater in the ischemic LAD than in the nonischemic LCX in the control group (Fig. 7a, $p < 0.01$). This Rho-kinase activation was significantly suppressed by hydroxyfasudil in the ischemic LAD (Fig. 7a, $p < 0.01$). Expression of eNOS protein in the ischemic endocardium of the LAD area (as determined by Western blotting) was significantly decreased ($79 \pm 4\%$, $p < 0.05$) compared with the nonischemic endocardium of the LCX area ($100 \pm 7\%$), which was also improved by hydroxyfasudil ($105 \pm 6\%$) (Fig. 7b, $p < 0.05$). There was no significant difference in the eNOS expression in the epicardium between the LAD and LCX area (Fig. 7c).

Effect of Rho-kinase inhibition on I/R-induced myocardial infarct size. Ischemia-reperfusion injury caused myocardial infarct area that was approximately 50% of the left ventricular risk area, and intracoronary L-NMMA did not further increase the I/R-induced infarction size (Fig. 8a). Intracoronary pretreatment with hydroxyfasudil markedly reduced the infarct size ($p < 0.01$ vs. control), and this beneficial effect of hydroxyfasudil was significantly attenuated by L-NMMA (Fig. 8a $p < 0.01$). In the control group, there was an inverse relation between the infarct area and collateral blood flow measured by microsphere technique ($r = 0.93$, $p < 0.01$), and hydroxyfasudil significantly shifted the regression line downward as compared with the control group ($p < 0.01$), that is, smaller infarct size for a given collateral flow (Fig. 8b).

DISCUSSION

The major findings of the present in vivo study in the canine coronary microcirculation were that: 1) a specific Rho-kinase inhibitor hydroxyfasudil preserved the endothelium-dependent coronary vasodilator responses after coronary I/R injury, 2) hydroxyfasudil also reduced myocardial infarct size, and 3) NO may be involved in those cardiovascular protective effects of hydroxyfasudil. To the best of our knowledge, this is the first report that demonstrates the usefulness of a Rho-kinase inhibitor to prevent coronary I/R injury in vivo.

Validations of experimental model and methodology. On the basis of the previous reports (4,12,20), we chose the adequate dose of hydroxyfasudil, acetylcholine, papaverine, and L-NMMA to examine the effects of the Rho-kinase inhibition, endothelium-dependent and -independent vasodilator responses, and inhibition of NO synthesis on coronary vascular responses before and after coronary I/R, respectively. The methodologic validity of the present study has been confirmed previously (15). After 60 to 90 min of ischemia, ultrastructural damage of coronary endothelium was observed particularly in the subendocardium in the present study, a consistent finding to the previous study (21).

Hydroxyfasudil as a specific Rho-kinase inhibitor in the coronary microcirculation in vivo. Shimokawa et al. (11) have recently demonstrated that hydroxyfasudil is a specific Rho-kinase inhibitor that markedly inhibits coronary vasospastic responses in a porcine model; its inhibitory effect on Rho-kinase is 100 times greater than on protein kinase C and

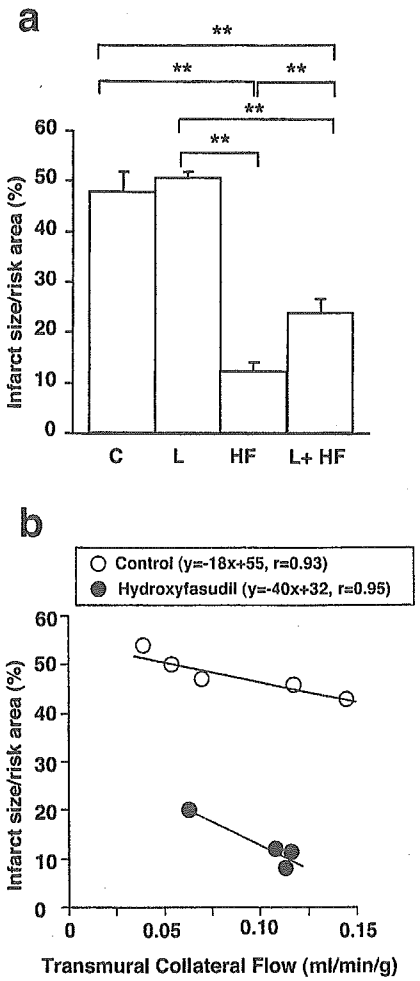

Figure 8. **(a)** Ischemia/reperfusion (I/R)-induced LV infarct size in dogs in vivo. Hydroxyfasudil significantly reduced the I/R-induced LV infarct size. The beneficial effect of hydroxyfasudil was partially attenuated by L-NMMA, while L-NMMA alone did not significantly increase the infarct size. Number of animals used was each 7 for C, HF, and L + HF, and 4 for L. C = control; L = L-NMMA; HF = hydroxyfasudil. **$p < 0.01$. **(b)** Plot of infarct size expressed as a percentage of the risk area and regional collateral flow during ischemia. In the control group, there was an inverse relation between infarct area and collateral flow measured by microsphere ($r = 0.93$, $p < 0.01$), and hydroxyfasudil significantly shifted the regression line downward as compared with the control group ($p < 0.01$). Number of animals used was five for control conditions and four for hydroxyfasudil.

1,000 times greater on myosin light-chain kinase. Hydroxyfasudil has potent vasodilator effects on coronary arteries through inhibition of Rho-kinase-mediated phosphorylations of myosin light chains (11). In the present study, intracoronary hydroxyfasudil caused coronary microvascular vasodilation in a dose-dependent manner in vivo, and its vasodilator effect was greater in arterioles than in small arteries (Fig. 2). Hydroxyfasudil suppressed the serotonin-induced vasoconstriction of small arteries, whereas it enhanced the serotonin-induced vasodilation of arterioles in vivo (Fig. 3). This finding is in accordance with the hypothesis that the calcium sensitization of vascular smooth-muscle cells mediated by Rho-kinase plays a key role in the molecular mechanisms of coronary hyperconstriction (12). Furthermore, in the present study, intracoronary L-NMMA significantly attenuated serotonin-induced coronary vasodilator responses, which were improved by hydroxyfasudil, indicating an involvement of NO-mediated mechanism in the beneficial effects of the Rho-kinase inhibitor. Lamping et al. (22) demonstrated that coronary vascular response to serotonin is determined by a balance between 5-HT_1 receptor-mediated dilatation of coronary arterioles and 5-HT_2 receptor-mediated vasoconstriction of small coronary arteries. Inhibition of NO synthase enhances coronary vasoconstriction to serotonin in both-sized arteries. Our present results are in agreement with those of Lamping et al. The beneficial vasodilator effect of hydroxyfasudil on coronary vascular response to serotonin is mediated by its action on both vascular smooth muscle and the endothelium as shown in Figure 3. Thus, it is possible that the beneficial effect of Rho-kinase blockade with hydroxyfasudil is mediated by its action on both vascular smooth muscle and the endothelium (22). Serotonin released by aggregating platelets has been implicated for coronary vasospasm in the presence of damaged vascular endothelium (5,23).

Beneficial effects of a Rho-kinase inhibitor on coronary I/R injury. In the present study, hydroxyfasudil exerted beneficial effects on I/R-induced endothelial injury in the canine coronary microcirculation in vivo through the NO-dependent mechanism (Figs. 4 and 5). This dose of hydroxyfasudil (100 μg/kg) selectively inhibits Rho-kinase activity and effectively prevents serotonin-induced coronary hyperconstriction. Recent studies have demonstrated that cGMP-dependent protein kinase inhibits RhoA phosphorylation by inhibiting the membrane binding of RhoA, in which the NO-mediated mechanism may inhibit the RhoA/Rho-kinase pathway (24–26). It was previously demonstrated that statins attenuate I/R injury of the heart and the brain in rats and mice, demonstrating the Rho-mediated and NO-dependent protective effect of statins (27,28). Hydroxyfasudil also inhibits the production of superoxide anions in neutrophils (29) and various chemoattractant-induced migration of those cells (14) in a canine model of cerebral ischemia. Furthermore, treatment with hydroxyfasudil in human saphenous vein endothelial cells reversed the hypoxia-induced decrease in eNOS activity as examined by the citrulline conversion assay and 4,5-diaminofluorescein diacetate fluorescence method (13). In the present study, I/R increased Rho-kinase activity, and hydroxyfasudil significantly inhibited the Rho-kinase activation. These findings suggest that NO is involved in the protective effect of hydroxyfasudil with an increase in eNOS activity and a decrease in Rho-kinase activity during reperfusion injury.

In the present study, the vasodilator effects of hydroxyfasudil were significantly attenuated by L-NMMA (Figs. 3 and 4). The eNOS expression was decreased in the ischemic area of the endocardium compared with that of the epicardium under control conditions, which was improved by hydroxyfasudil (Fig. 7). We have previously demonstrated that endocardial arteriolar dilation during reactive hyperemia is more sensitive to L-NMMA than epicardial arte-

Table 1. Hemodynamics During Myocardial Ischemia-Reperfusion Injury in Dogs

		Before I/R			After I/R		
	n	Baseline	ACh	Papaverine	Baseline	ACh	Papaverine
MBP (mm Hg)							
Control	7	91 ± 4	90 ± 6	92 ± 5	89 ± 4	89 ± 5	92 ± 6
L-NMMA	4	88 ± 8	86 ± 5	91 ± 7	86 ± 4	86 ± 4	85 ± 4
Hydroxyfasudil	7	92 ± 9	92 ± 8	93 ± 8	93 ± 6	90 ± 6	91 ± 7
L-NMMA + hydroxyfasudil	7	89 ± 6	89 ± 5	89 ± 5	91 ± 8	87 ± 10	89 ± 9
Heart rate (beats/min)							
Control	7	151 ± 5	156 ± 3	155 ± 3	155 ± 5	153 ± 5	152 ± 5
L-NMMA	4	147 ± 7	149 ± 8	149 ± 8	145 ± 11	146 ± 11	145 ± 11
Hydroxyfasudil	7	152 ± 7	151 ± 8	148 ± 8	148 ± 7	149 ± 7	150 ± 7
L-NMMA + hydroxyfasudil	7	151 ± 6	152 ± 6	151 ± 6	154 ± 6	151 ± 6	153 ± 7

Results are expressed as mean ± SEM.
ACh = acetylcholine; I/R = ischemia/reperfusion; MBP = mean blood pressure.

riolar dilation (30). These findings indicate that the perfusion of the endocardium is more dependent on NO than that of the epicardium and that endothelial damage after I/R in arterioles may be greater in the endocardium than in the epicardium.

In the present study, hydroxyfasudil exerted cardiovascular protective effects on coronary I/R injury, as did preconditioning (31,32). However, the mechanism by which hydroxyfasudil and preconditioning protect coronary I/R injury appears to be different. Endogenous NO does not alter the infarct size after I/R and is not involved in the protective mechanism of preconditioning in pigs or rabbits (33,34). It has been suggested that preconditioning preserves myocardial creatine phosphate and intracellular pH (35). Furthermore, ischemic preconditioning increases adenosine production and activates protein kinase C, which also enhances adenosine production during I/R injury.

In the present study, hydroxyfasudil significantly reduced myocardial infarct size with increment of coronary collateral blood flow, at least in part, thorough the NO-mediated mechanism (Fig. 8). Shimokawa et al. (11) demonstrated that hydroxyfasudil inhibits both MLC mono- and diphosphorylations. Satoh et al. (14) showed that hydroxyfasudil also protects the brain from ischemic injury through inhibition of superoxide production and neutrophil infiltration. Mohri et al. (36) demonstrated that fasudil suppresses coronary microvascular spasm in patients with microvascular angina. Wolfrum et al. (37) recently demonstrated that inhibiting Rho-kinase has cardioprotective effects to reduce infarct size by activating phosphatidylinositol 3-kinase/protein kinase Akt/eNOS pathways. All these mechanisms may be involved in the beneficial effects of hydroxyfasudil on the I/R-induced myocardial injury.

Hydroxyfasudil increases blood supply to the ischemic region of the myocardium and prevents I/R-induced myocardial injury. Furthermore, it has been recently demonstrated that an estrogen receptor modulator, raloxifene, also reduces I/R-induced myocardial infarct size, whereas an inhibitor of NO synthesis (L-NAME) or a blocker of calcium-activated K^+ channels (charybdotoxin) partly attenuates the effect of raloxifene (19). These results suggest that cardioprotective effects of those inhibitors may be mediated in part by the compensatory effects of NO and endothelium-derived hyperpolarizing factor (20). Several studies using NO synthase inhibitors (38,39) or eNOS-deficient mice (40) demonstrated an increase in infarct size after I/R. The effect of NO synthesis inhibition on the infarct size might be species- and dose-dependent.

Clinical implications and conclusions. The present study has demonstrated for the first time that hydroxyfasudil, a specific Rho-kinase inhibitor, has NO-dependent cardiovascular protective effects on coronary I/R injury in vivo. Rho-kinase inhibitor has also an antianginal effect in a canine model of angina (41), patients with effort angina (42), and those with vasospastic angina (43). Moreover, it has been recently reported that hydroxyfasudil may be effective for the treatment of pulmonary hypertension (44). Indeed, Rho-kinase inhibitors may be useful for the treatment of a wide range of cardiovascular diseases (10). The present study suggests that Rho-kinase inhibitors may also be useful for the treatment of coronary I/R injury in humans.

Acknowledgment

We thank Y. Matsuo for excellent technical assistance in this study.

Reprint requests and correspondence: Dr. Toyotaka Yada, Kawasaki Medical School, 577 Matsushima, Kurashiki, Okayama, 701-0192, Japan. E-mail: yada@me.kawasaki-m.ac.jp.

REFERENCES

1. Vanbenthuysen PJ, McMurtry IF, Horwitz LD, et al. Reperfusion after acute coronary occlusion in dogs impairs endothelium-dependent relaxation to acetylcholine and augments contractile reactivity in vitro. J Clin Invest 1987;79:265–74.
2. Pearson PJ, Schaff HV, Vanhoutte PM, et al. Acute impairment of endothelium-dependent relaxations to aggregating platelets following reperfusion injury in canine coronary arteries. Circ Res 1990; 67:385–93.
3. Mehta JL, Nichols WW, Donnelly WH, et al. Impaired canine coronary vasodilator response to acetylcholine and bradykinin after occlusion-reperfusion. Circ Res 1989;64:43–54.

4. Defily DV, Chilian WM. Preconditioning protects coronary arteriolar endothelium from ischemia-reperfusion injury. Am J Physiol 1993; 265:H700–6.
5. Vanhoutte PM, Shimokawa H. Endothelium-derived relaxing factor and coronary spasm. Circulation 1989;80:1–9.
6. Korthuis RJ, Granger DN, Townsley MI, et al. The role of oxygen-derived free radicals in ischemia-induced increases in canine skeletal muscle vascular permeability. Circ Res 1985;57:599–609.
7. Olafsson B, Forman MB, Puett DW, et al. Reduction of reperfusion injury in the canine preparation by intracoronary adenosine: importance of the endothelium and the no-reflow phenomenon. Circulation 1987;76:1135–45.
8. Lamping KG, Marcus ML, Dole WP. Removal of endothelium potentiates canine large coronary artery constrictor response to 5-hydroxytryptamine in vivo. Circ Res 1985;57:46–54.
9. Cohen RA, Shepherd JT, Vanhoutte PM. 5-hydroxytryptamine can mediate endothelium-dependent relaxation of coronary arteries. Am J Physiol 1983;245:H1077–80.
10. Shimokawa H. Rho-kinase as a novel therapeutic target in treatment of cardiovascular diseases. J Cardiovasc Pharmacol 2002;39:319–27.
11. Shimokawa H, Seto M, Katsumata N, et al. Rho-kinase-mediated pathway induces enhanced myosin light chain phosphorylations in a swine model of coronary artery spasm. Cardiovasc Res 1999;43: 1029–39.
12. Kandabashi T, Shimokawa H, Miyata K, et al. Inhibition of myosin phosphatase by upregulated Rho-kinase plays a key role for coronary artery spasm in a porcine model with interleukin-1β. Circulation 2000;101:1319–23.
13. Takemoto M, Sun J, Hiroki J, et al. Rho-kinase mediates hypoxia-induced downregulation of endothelial nitric oxide synthase. Circulation 2002;106:57–62.
14. Satoh S, Utsunomiya T, Tsurui K, et al. Pharmacological profile of hydroxy fasudil as a selective Rho-kinase inhibitor on ischemic brain damage. Life Sci 2001;69:1441–53.
15. Yada T, Hiramatsu O, Kimura A, et al. In vivo observation of subendocardial microvessels of the beating porcine heart using a needle-probe videomicroscope with a CCD camera. Circ Res 1993; 72:939–46.
16. Mori HS, Haruyama Y, Shinozaki H, et al. New nonradioactive microspheres and more sensitive X-ray fluorescence to measure regional blood flow. Am J Physiol 1992;263:H1946–57.
17. Laufs U, Fata VL, Liao JK. Inhibition of 3-hydroxy-3-methylglutaryl (HMG)-CoA reductase blocks hypoxia-mediated down-regulation of endothelial nitric oxide synthase. J Biol Chem 1997;272:31725–9.
18. Katsura M, Mohri Y, Shuto K, et al. Up-regulation of L-type voltage-dependent calcium channels after long term exposure to nicotine in cerebral cortical neurons. J Biol Chem 2002;277:7979–88.
19. Ogita H, Node K, Asanuma H, et al. Amelioration of ischemia- and reperfusion-induced myocardial injury by the selective estrogen receptor modulator, raloxifene, in the canine heart. J Am Coll Cardiol 2002;40:998–1005.
20. Yada T, Shimokawa H, Hiramatsu O, et al. Hydrogen peroxide, an endogenous EDHF, plays an important role in coronary autoregulation in vivo. Circulation 2003;107:1040–5.
21. Ehring T, Krajcar M, Baumgart D, et al. Cholinergic and α-adrenergic coronary constriction with increasing ischemia-reperfusion injury. Am J Physiol 1995;268:H886–94.
22. Lamping KG. Enhanced contractile mechanisms in vasospasm: is endothelial dysfunction the whole story? Circulation 2002;105: 1520–2.
23. Golino P, Ashton JH, Buja LM, et al. Local platelet activation causes vasoconstriction of large epicardial canine arteries in vivo: thromboxane A2 and serotonin are possible mediators. Circulation 1989;79: 154–66.
24. Chitaley K, Webb RC. Nitric oxide induces dilation of rat aorta via inhibition of Rho-kinase signaling. Hypertension 2002;39:438–42.
25. Sauzeau V, Le Jeune H, Cario-Toumaniantz C. Cyclic GMP-dependent protein kinase signaling pathway inhibits RhoA-induced Ca^{++} sensitization of contraction in vascular smooth muscle. Biol Chem 2000;275:21722–9.
26. Sawada N, Itoh H, Yamashita J, et al. Cyclic GMP-dependent protein kinase phosphorylates and inactivates RhoA. Biochem Biophys Res Commun 2001;280:798–805.
27. Ikeda Y, Lindon HY, Lefer AM. Rosuvastatin, a new HMG-CoA reductase inhibitor, protects ischemic reperfused myocardium in normocholesterolemic rats. J Cardiovasc Pharmacol 2003;41:649–56.
28. Amin-Hanjani S, Stagliano NE, Yamada M, et al. Mevastatin, an HMG-CoA reductase inhibitor, reduces stroke damage and upregulates endothelial nitric oxide synthase in mice. Stroke 2001;32:980–6.
29. Arai M, Sasaki Y, Nozawa R. Inhibition by the protein kinase inhibitor HA1077 of the activation of NADPH oxidase in human neutrophils. Biochem Pharmacol 1993;46:1487–90.
30. Yada T, Hiramatsu O, Kimura A, et al. Direct in vivo observation of subendocardial arteriolar responses during reactive hyperemia. Circ Res 1995;77:622–31.
31. Murry CE, Jennings RB, Reimer KA. Preconditioning with ischemia: a delay of lethal cell injury in ischemic myocardium. Circulation 1986;74:1124–36.
32. Cohen MV, Liu GS, Downey JM. Preconditioning causes improved wall motion as well as smaller infarcts after transient coronary occlusion in rabbits. Circulation 1991;84:341–9.
33. Post H, Schulz R, Behrends M, et al. No involvement of endogenous nitric oxide in classical ischemic preconditioning in swine. J Mol Cell Cardiol 2000;32:725–33.
34. Nakano A, Liu GS, Heusch G. Exogenous nitric oxide can trigger a preconditioning state through a free radical mechanism, but endogenous nitric oxide is not a trigger of classical ischemic preconditioning. J Mol Cell Cardiol 2000;32:1159–67.
35. Kida M, Fujiwara H, Ishida M, et al. Ischemic preconditioning preserves creatine phosphate and intracellular pH. Circulation 1991; 84:2495–503.
36. Mohri M, Shimokawa H, Hirakawa Y, et al. Rho-kinase inhibition with intracoronary fasudil prevents myocardial ischemia in patients with coronary microvascular spasm. J Am Coll Cardiol 2003;41:15–9.
37. Wolfrum S, Dendorfer A, Rikitake Y, et al. Inhibition of rho-kinase leads to rapid activation of phosphatidylinositol 3-kinase/protein kinase akt and cardiovascular protection. Arterioscler Thromb Vasc Biol 2004;24:1–6.
38. Williams MW, Taft CS, Ramnauth S, et al. Endogenous nitric oxide (NO) protects against ischaemia-reperfusion injury in the rabbit. Cardiovasc Res 1995;30:79–86.
39. Hoshida S, Yamashita N, Igarashi J, et al. Nitric oxide synthase protects the heart against ischemia-reperfusion injury in rabbits. J Pharmacol Exp Ther 1995;274:413–8.
40. Jones SP, Girod WG, Palazzo AJ, et al. Myocardial ischemia-reperfusion injury is exacerbated in absence of endothelial cell nitric oxide synthase. Am J Physiol 1999;276:H1567–73.
41. Utsunomiya T, Satoh S, Ikegaki I, et al. Antianginal effects of hydroxyfasudil, a Rho-kinase inhibitor, in a canine model of effort angina. Br J Pharmacol 2001;134:1724–30.
42. Shimokawa H, Hiramori K, Iinuma H, et al. Anti-anginal effect of fasudil, a Rho-kinase inhibitor, in patients with stable effort angina: a multicenter study. J Cardiovasc Pharmacol 2002;40:751–61.
43. Masumoto A, Mohri M, Shimokawa H, et al. Suppression of coronary artery spasm by the Rho-kinase inhibitor fasudil in patients with vasospastic angina. Circulation 2002;105:1545–7.
44. Abe K, Shimokawa H, Morikawa K, et al. Long-term treatment with a Rho-kinase inhibitor improves monocrotaline-induced fatal pulmonary hypertension in rats. Circ Res 2004;94:385–93.

Am J Physiol Heart Circ Physiol 288: H1444–H1450, 2005.
First published November 11, 2004; doi:10.1152/ajpheart.00266.2004.

Adrenomedullin enhances therapeutic potency of bone marrow transplantation for myocardial infarction in rats

Takafumi Fujii,[1] Noritoshi Nagaya,[2,3] Takashi Iwase,[2] Shinsuke Murakami,[2] Yoshinori Miyahara,[1] Kazuhiro Nishigami,[3] Hatsue Ishibashi-Ueda,[5] Mikiyasu Shirai,[1] Takefumi Itoh,[2] Kozo Ishino,[6] Shunji Sano,[6] Kenji Kangawa,[4] and Hidezo Mori[1]

Departments of [1]Cardiac Physiology, [2]Regenerative Medicine and Tissue Engineering, [3]Internal Medicine, [4]Biochemistry, and [5]Pathology, National Cardiovascular Center, Osaka; and [6]Department of Cardiovascular Surgery, Okayama University Medical School, Okayama, Japan

Submitted 18 March 2004; accepted in final form 19 October 2004

Fujii, Takafumi, Noritoshi Nagaya, Takashi Iwase, Shinsuke Murakami, Yoshinori Miyahara, Kazuhiro Nishigami, Hatsue Ishibashi-Ueda, Mikiyasu Shirai, Takefumi Itoh, Kozo Ishino, Shunji Sano, Kenji Kangawa, and Hidezo Mori. Adrenomedullin enhances therapeutic potency of bone marrow transplantation for myocardial infarction in rats. *Am J Physiol Heart Circ Physiol* 288: H1444–H1450, 2005. First published November 11, 2004; doi: 10.1152/ajpheart.00266.2004.—Adrenomedullin (AM), a potent vasodilator, induces angiogenesis and inhibits cell apoptosis through the phosphatidylinositol 3-kinase/Akt pathway. Transplantation of bone marrow-derived mononuclear cells (MNC) induces angiogenesis. We investigated whether infusion of AM enhances the therapeutic potency of MNC transplantation in a rat model of myocardial infarction. Immediately after coronary ligation, bone marrow-derived MNC (5×10^6 cells) were injected into the ischemic myocardium, followed by subcutaneous administration of 0.05 $\mu g \cdot kg^{-1} \cdot min^{-1}$ AM (AM-MNC group) or saline (MNC group) for 3 days. Another two groups of rats received subcutaneous administration of AM alone (AM group) or saline (control group). Hemodynamic and histological analyses were performed 4 wk after treatment. Cardiac infarct size was significantly smaller in the MNC and AM groups than in the control group. A combination of AM infusion and MNC transplantation demonstrated a further decrease in infarct size. Left ventricular (LV) maximum change in pressure over time and LV fractional shortening were significantly improved only in the AM-MNC group. AM significantly increased capillary density in ischemic myocardium, suggesting the angiogenic potency of AM. AM infusion plus MNC transplantation demonstrated a further increase in capillary density compared with AM or MNC alone. Although MNC apoptosis was frequently observed 72 h after transplantation, AM markedly decreased the number of terminal deoxynucleotidyl transferase-mediated dUTP nick-end labeling-positive cells among the transplanted MNC. In conclusion, AM enhanced the angiogenic potency of MNC transplantation and improved cardiac function in rats with myocardial infarction. This beneficial effect may be mediated partly by the angiogenic property of AM itself and by its antiapoptotic effect on MNC.

angiogenesis; apoptosis; mononuclear cell

DESPITE THE RECENT REMARKABLE progress in medical and surgical treatment for ischemic heart disease, this disease remains a major cause of death worldwide (5). Bone marrow-derived mononuclear cells (MNC) contain various kinds of cell lineages and numerous cytokines that contribute to neovascularization (1, 15). In fact, autologous transplantation of bone marrow cells has been shown to enhance angiogenesis and improve cardiac function in an animal model of cardiac ischemia (6, 9, 10). Recent human studies have demonstrated beneficial effects of transplanted MNC in patients with ischemic heart disease (23, 25). However, some patients fail to respond to this cell therapy. Thus a novel therapeutic strategy to enhance the angiogenic property of MNC is desirable.

Adrenomedullin (AM) is a potent vasodilator peptide that was originally isolated from human pheochromocytoma (8). We have shown that infusion of AM has beneficial hemodynamic and renal effects in patients with heart failure (17). On the other hand, AM has been shown to activate the phosphatidylinositol 3-kinase (PI3-kinase)/Akt-dependent pathway in vascular endothelial cells, which is considered to regulate multiple critical steps in angiogenesis including endothelial cell proliferation, migration, and capillary-like formation (14, 22). In fact, we have shown that AM gene transfer induces therapeutic angiogenesis in a rabbit model of hindlimb ischemia via activation of Akt (24). These findings suggest that AM may play an important role in the regulation of vascular regeneration. In addition, AM has been shown to exert an antiapoptotic effect on a variety of cells including vascular endothelial cells (7, 20). Taking these findings together, combination therapy with MNC transplantation and AM infusion may have additional or synergetic effects on therapeutic angiogenesis for the treatment of ischemic heart disease.

Thus the purposes of this study were *1*) to investigate whether infusion of AM enhances the angiogenic potency of MNC transplantation in a rat model of myocardial infarction, and *2*) to investigate the effects of AM on survival and differentiation of the transplanted MNC to examine the underlying mechanisms of the effects induced by AM.

MATERIALS AND METHODS

Animal model. Myocardial infarction was produced in male Lewis rats weighing 200–220 g by left coronary ligation. In brief, after rats were anesthetized by intraperitoneal injection of pentobarbital sodium (30 mg/kg body wt), they were ventilated artificially. The heart was exposed via left thoracotomy, and the left coronary artery was ligated 2–3 mm from its origin between the pulmonary artery conus and the left atrium using a 6-0 proline suture. Finally, the heart was restored to its normal position, and the chest was closed. The Animal Care Committee of the National Cardiovascular Center approved this experimental protocol.

Address for reprint requests and other correspondence: N. Nagaya, Dept. of Regenerative Medicine and Tissue Engineering, National Cardiovascular Center Research Institute, 5-7-1 Fujishirodai, Suita, Osaka 565-8565, Japan (E-mail: nnagaya@ri.ncvc.go.jp).

The costs of publication of this article were defrayed in part by the payment of page charges. The article must therefore be hereby marked "*advertisement*" in accordance with 18 U.S.C. Section 1734 solely to indicate this fact.

Preparation of MNC. After Lewis rats were killed, bone marrow from the femur and tibia was collected and put in PBS. Marrow cells were loaded on a 1.077 gradient of Ficoll (Lymphoprep; Nycomed Pharma, Oslo, Norway) and centrifuged at 1,500 rpm for 20 min. The cells were then washed with 10 ml PBS to remove the Ficoll and centrifuged at 2,000 rpm for 10 min. The cells were finally suspended in PBS at a concentration of 5×10^6 cells in 50 μl PBS for transplantation. Fluorescence-activated cell sorting analysis demonstrated that 22 ± 1% of MNC were positive for lectin from ulex europaeus (UEA)-1 lectin (Sigma, St. Louis, MO).

MNC transplantation and AM infusion. Transplantation of bone marrow-derived MNC and/or 3-day infusion of AM was performed immediately after coronary ligation. MNC (5×10^6 cells in 50 μl PBS) were injected into the myocardium at five points in the border zone surrounding the infarct by using a 27-gauge needle. Recombinant human AM (0.05 $\mu g \cdot kg^{-1} \cdot min^{-1}$) was subcutaneously administered by using an osmotic minipump (model 2004; Alza, Palo Alto, CA) for 3 days. The pump was positioned in a pocket constructed in the subcutaneous tissue just below the subscapular region. For control, 5% glucose was infused in a similar manner in the rats receiving coronary ligation. This protocol resulted in the creation of four groups: *1*) AM infusion plus MNC transplantation (AM-MNC group, $n = 15$), *2*) vehicle infusion plus MNC transplantation (MNC group, $n = 14$), *3*) AM infusion plus PBS injection (AM group, $n = 14$), and *4*) vehicle infusion plus PBS injection (control group, $n = 13$).

Echocardiographic studies. Echocardiographic studies were performed 4 wk after surgery using a 7.5-MHz phased-array transducer (model HP SONOS 5500; Hewlett-Packard, Andover, MA). Rats were anesthetized by intraperitoneal injection of pentobarbital sodium (30 mg/kg body wt) as a supplement to maintain mild anesthesia. M-mode tracings were obtained at the level of the papillary muscles. Anterior and posterior end-diastolic wall thickness, left ventricular (LV) end-diastolic and end-systolic dimension, and LV fractional shortening were measured from three consecutive cardiac cycles by the American Society for Echocardiology leading-edge method (21).

Cardiac catheterization. Cardiac catheterization was performed 4 wk after surgery. Rats were anesthetized with intraperitoneal pentobarbital and placed on a heating pad to maintain body temperature at 37–38°C throughout the study. A 1.5 Fr micronanometer-tipped catheter was inserted in the right carotid artery for measurement of heart rate and mean arterial pressure. The catheter was then advanced into the LV for measurement of LV end-diastolic pressure and then replaced with a thermomicroprobe for measurements of cardiac output. These hemodynamic variables were measured with a pressure transducer (UFI, Morro Bay, CA) connected to a polygraph and recorded with a thermal recorder (model 7758 B system; Hewlett-Packard).

Infarct size measurement. After completion of hemodynamic measurements, the heart was arrested by an injection of 2 mmol KCl through the carotid artery, and the cardiac ventricles were excised. The size of myocardial infarction was determined by a previously described method (2). In brief, incisions were made in the LV so that the tissue could be pressed flat. The circumference of the entire flat LV and the visualized infarcted area, as judged from both the epicardial and endocardial sides, was outlined on a clear plastic sheet. The difference in weight between the two marked areas on the sheet was used to determine infarction size and was expressed as a percentage of LV surface area.

Histological analysis of microvessel density. LV myocardium was fixed in 10% formalin. Three cross sections of the LV, cut from apex to base, were obtained from individual rats for comparison among four groups ($n = 5$ each). They were embedded in paraffin and stained with Masson's trichrome for measurement of interstitial fibrosis. In other rats ($n = 5$ each), LV myocardium was embedded in optimum cutting temperature (OCT) compound (Sakura Finetechnical, Tokyo, Japan), snap frozen in liquid nitrogen, and cut into 5-μm-thick sections. Tissue sections were stained for alkaline phosphatase with an indoxyltetrazolium method to detect capillary endothelial cells ($n = 5$ in each group). The number of capillary vessels was counted in the peri-infarct area (a 1.0-mm band next to the scar) excluding scar region using a light microscope at a magnification of ×200. The numbers in five high-power fields in each rat were averaged and expressed as the number of capillary vessels. These morphometric studies were performed by two examiners who were blinded to treatment.

Detection of MNC apoptosis. To examine the antiapoptotic effect of AM on transplanted MNC, red fluorescence-labeled MNC were transplanted into ischemic myocardium in rats with ($n = 5$) and without ($n = 5$) AM infusion. Before implantation into the ischemic heart, suspended MNC were labeled with fluorescent dyes with a PKH26 (Red Fluorescent Cell Linker Kit; Sigma), as reported previously (13). AM was subcutaneously administered by using a minipump for 3 days. Rats were killed 72 h after MNC transplantation. The LV was enucleated, and muscle samples were embedded in OCT compound and snap frozen in liquid nitrogen for the detection of apoptosis. Serial sections of the heart were stained by terminal deoxynucleotidyl transferase-mediated dUTP nick-end labeling (TUNEL) for apoptosis using an in situ apoptosis detection kit (model S7111 Apoptag Fluorescein Kit; Intergen). Apoptosis of transplanted MNC was also evaluated by the detection of cleaved caspase-3-positive cells. In brief, the frozen tissue sections were incubated with anticleaved caspase-3 antibody (Cell Signaling), followed by incubation with FITC-conjugated IgG antibody (BD Pharmingen, San Diego, CA). The number of TUNEL/PKH26 double-positive cells and caspase-3/PKH26 double-positive cells was counted in 10 fields of each rat using a confocal microscopy (Fluoview model 500; Olympus, Tokyo, Japan).

The antiapoptotic effect of AM on MNC was also evaluated by in vitro TUNEL assay. MNC were plated on 12-well plates (1×10^6 cells per well) and cultured in serum-free medium for 24 h with control buffer, AM (1×10^{-7} M), or AM plus wortmannin, a PI3-kinase inhibitor (50 nM). Randomly selected microscopic fields ($n = 10$) were evaluated for calculating the ratio of TUNEL-positive cells to total cells.

Monitoring of implanted MNC in ischemic heart. Additional rats were used to examine whether transplanted MNC differentiate into endothelial cells, cardiomyocytes, vascular smooth muscle cells, or macrophages in the ischemic heart. PKH26 (red fluorescence)-labeled MNC were injected into the ischemic heart in rats with ($n = 8$) and without ($n = 8$) AM infusion. These subgroups of rats were killed 4 wk after coronary ligation. To identify vascular endothelial cells in vivo, FITC-labeled UEA-1 lectin was intravenously administered 30 min before the rats were killed ($n = 5$ in each group). The LV was enucleated, and muscle samples were then embedded in OCT compound, snap frozen in liquid nitrogen, and cut into sections. Sections were counterstained with 4′,6′-diamidino-2-phenylindole (DAPI) to detect nuclei. The number of DAPI/PKH26 double-positive cells and lectin-positive cells in the peri-infarct area was counted in 10 fields of each rat using a confocal microscopy. Frozen sections from other rats ($n = 3$ in each group) were incubated with mouse anticardiac troponin T (Novocastra, Newcastle, UK), anti-α-smooth muscle actin antibody (Dako, Copenhagen, Denmark), and anti-ED1 antibody (Serotec, Oxford, UK), followed by incubation with FITC-conjugated IgG antibody. In other rats (MNC group, $n = 5$; AM-MNC group, $n = 5$), the cardiac muscle from base to apex was transversely cut into 6-μm slices to calculate the number of transplanted MNC present within the heart 4 wk after transplantation. These morphometric studies were performed by two examiners who were blinded to treatment.

Statistical analysis. Numerical values were expressed as means ± SE. Comparisons of parameters among the four groups were performed by one-way ANOVA, followed by Newman-Keuls test for unpaired data. Comparisons of parameters between two groups were made by unpaired Student's *t*-test. A value of $P < 0.05$ was considered significant.

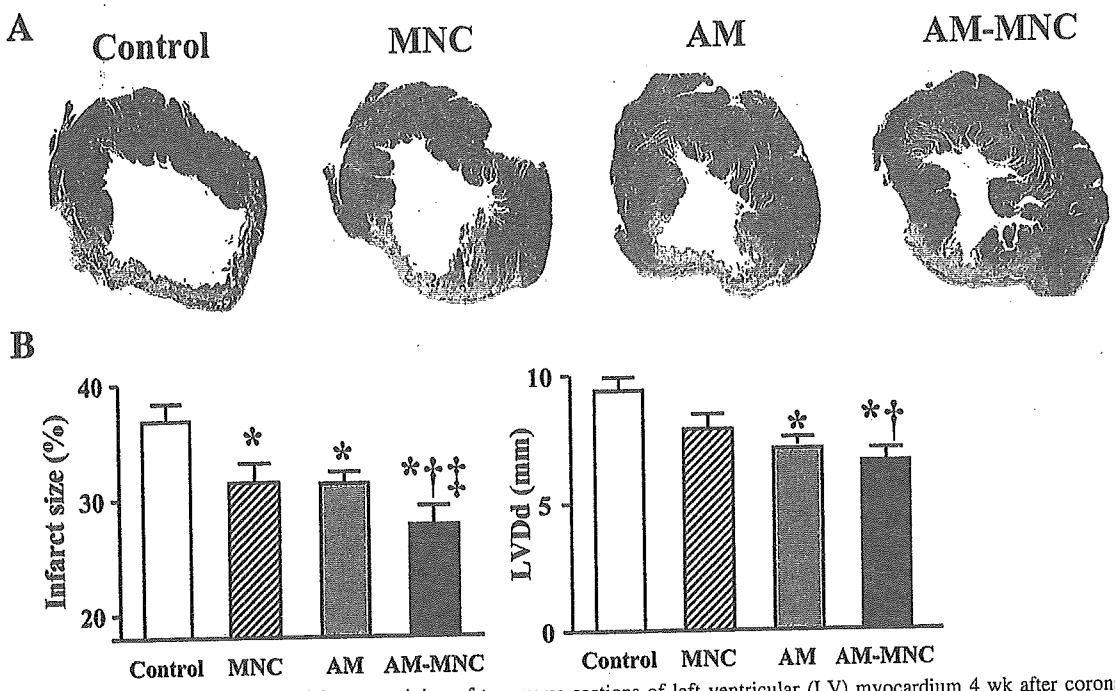

Fig. 1. *A*: representative examples of Masson trichrome-staining of transverse sections of left ventricular (LV) myocardium 4 wk after coronary ligation. *B*: quantitative analysis of infarct size and LV chamber size. Infarcted area and LV end-diastolic diameter (LVDd) of the adrenomedullin-mononuclear cell (AM-MNC) group were significantly smaller than those of the other groups. Values are means ± SE. *$P < 0.05$ vs. control; †$P < 0.05$ vs. MNC; ‡$P < 0.05$ vs. AM.

RESULTS

Infarct size and ventricular weight. Moderate-to-large infarcts were observed in the control group after coronary ligation (Fig. 1). However, infarct size was smaller in the MNC, AM, and AM-MNC groups than in the control group. In particular, it was very small in the AM-MNC group. Quantitative analysis also demonstrated that cardiac infarct size in the AM-MNC group was smallest among the four groups. Right ventricular weight was significantly lower in the AM and AM-MNC groups than that in the control group (Table 1). LV weight did not significantly differ among the four groups.

Echocardiographic findings. LV diastolic dimension was smallest in the AM-MNC group, followed by the AM, MNC, and control groups (Fig. 1). LV fractional shortening in the AM-MNC group was also higher than that in the control, MNC, and AM groups (Table 2). Diastolic thickness of the anterior wall was significantly attenuated in the MNC, AM, and AM-MNC groups compared with the control group.

Hemodynamics. Cardiac output in the AM-MNC group was significantly higher than that in the control, MNC, and AM groups (Fig. 2). LV end-diastolic pressure in the MNC, AM, and AM-MNC groups was significantly lower than that in the control group. LV maximum change in pressure over time (d*P*/d*t*) in the MNC and AM-MNC group were significantly higher than that in the control group. Similarly, LV minimum d*P*/d*t* was significantly decreased only in the AM-MNC group.

Capillary density. Alkaline phosphatase staining of ischemic myocardium showed marked augmentation of neovascularization in the MNC, AM, and AM-MNC groups compared with the control group (Fig. 3*A*). Quantitative analysis demonstrated that capillary density was significantly higher in the AM-MNC group than in the MNC and AM groups (Fig. 3*B*). Cartilage, bone, or fat was not observed in the transplanted area. No tumor-like cells were seen.

Antiapoptotic effect of AM on MNC. Red fluorescence-labeled MNC were detected in each recipient heart 72 h after transplantation (Fig. 4). TUNEL-positive cells were frequently observed in the MNC group. In contrast, these apoptotic cells

Table 1. *Physiological profiles of four experimental groups*

	Control	MNC	AM	AM-MNC
Number	13	14	14	15
Body weight, g	274±3	285±5	287±3	305±4*
Heart rate, bpm	410±24	404±30	398±33	387±36
MAP, mmHg	101±11	104±13	103±9	116±14*
LV wt/body wt, g/kg	2.4±0.2	2.5±0.2	2.6±0.1	2.5±0.2
RV wt/body wt, g/kg	1.1±0.1	0.9±0.1	0.8±0.1*	0.7±0.1*

Values are means ± SE; number is number of rats in each group. Control group, myocardial infarction rats given vehicle; MNC group, those given mononuclear cells; AM, those given adrenomedullin; AM-MNC, those given AM and MNC; MAP, mean arterial pressure; LV, left ventricle; RV, right ventricle. *$P < 0.05$ vs. control.

Table 2. *Echocardiographic findings*

	Control	MNC	AM	AM-MNC
LVDd, mm	9.9±0.2	8.3±0.3	7.3±0.2*	6.9±0.3*†
LVDs, mm	8.4±0.3	6.6±0.4	5.8±0.2*	5.1±0.2*
%FS, %	14±1	22±1*	21±1*	26±1*†‡
AWT diastole, mm	1.0±0.2	1.3±0.3*	1.3±0.3*	1.4±0.4*
PWT diastole, mm	1.5±0.5	2.2±0.4	2.1±0.4	2.2±0.4

Values are means ± SE. LVDd, LV diastolic dimension; LVDs, LV systolic dimension; %FS, LV fractional shortening; AWT, anterior wall thickness; PWT, posterior wall thickness. *$P < 0.05$ vs. control; †$P < 0.05$ vs. MNC; ‡$P < 0.05$ vs. AM.

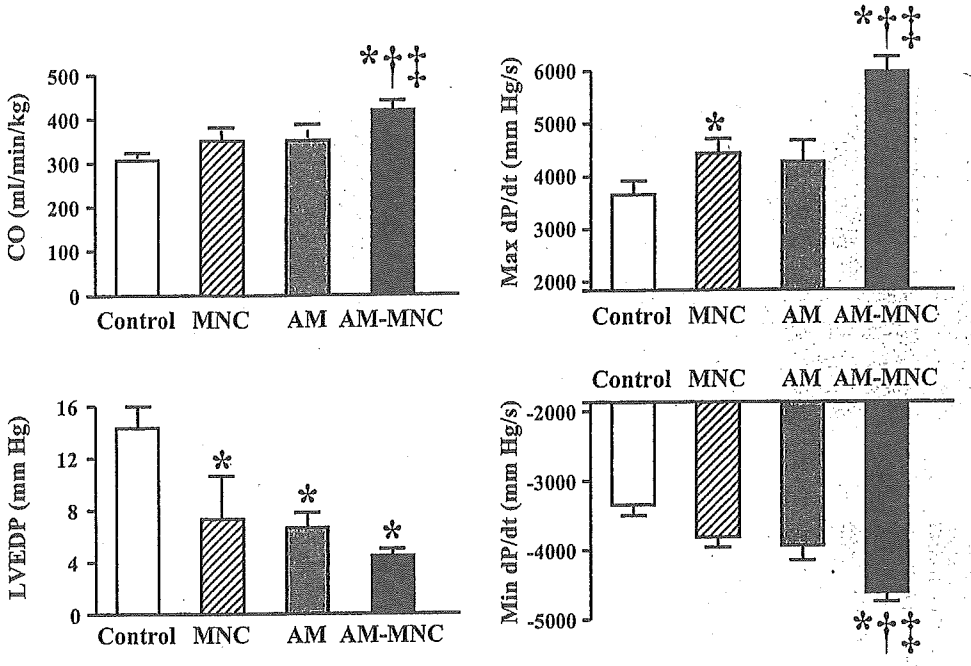

Fig. 2. Effects of AM infusion and MNC transplantation on hemodynamic parameters. CO, cardiac output; LVEDP, LV end-diastolic pressure; Max dP/d*t*, LV maximum change in pressure over time; Min dP/d*t*, LV minimum dP/d*t*. Values are means ± SE. *$P < 0.05$ vs. control; †$P < 0.05$ vs. MNC; ‡$P < 0.05$ vs. AM.

were hardly detected in the AM-MNC group. Semiquantitative analysis demonstrated that the number of TUNEL-positive MNC was significantly lower in the AM-MNC group than in the MNC group. Similarly, the number of caspase-3-positive MNC was significantly lower in the AM-MNC group than in the MNC group. These results suggest that infusion of AM inhibits apoptosis of transplanted MNC.

In vitro, serum starvation induced MNC apoptosis. When incubated in the presence of AM (1×10^{-7} M), the percentage of TUNEL-positive cells decreased significantly (19 ± 1 to 9 ± 1%, $P < 0.05$). However, pretreatment with wortmannin, a PI3-kinase inhibitor, diminished the antiapoptotic effect of AM (17 ± 1%).

Differentiation of MNC into endothelial lineage. Four weeks after transplantation, fluorescence-labeled transplanted cells

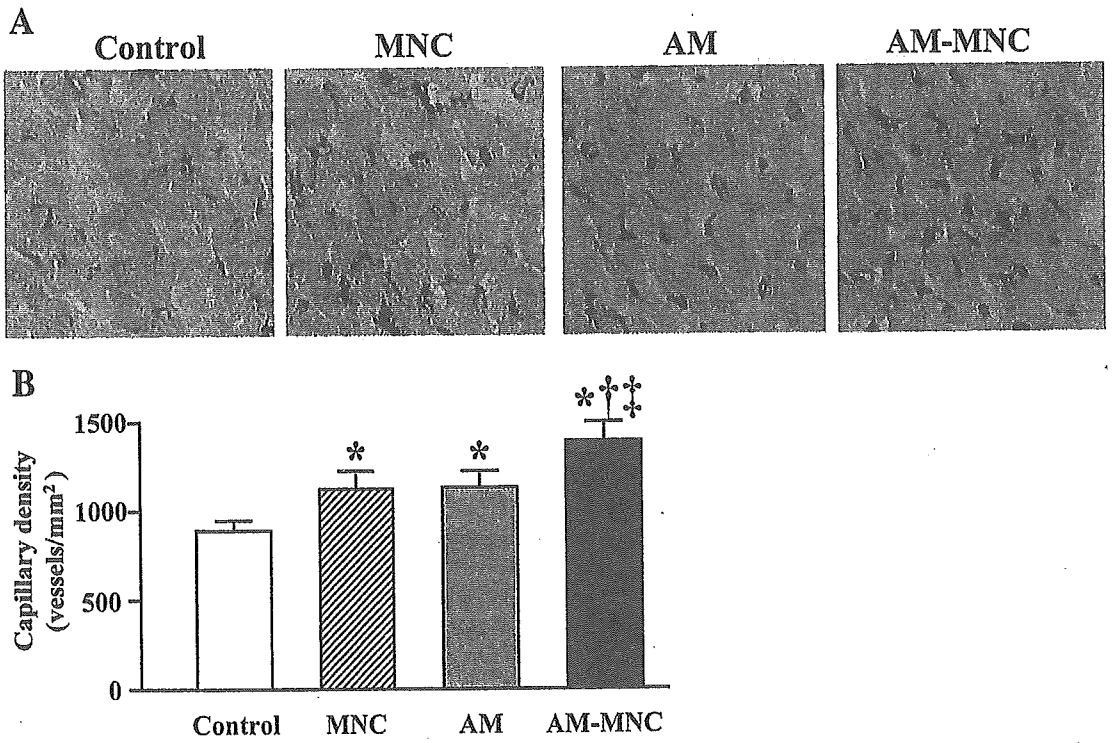

Fig. 3. *A*: representative examples of alkaline phosphatase staining in peri-infarct area. A combination of AM infusion and MNC transplantation markedly induced myocardial neovascularization. Magnification, ×200. *B*: quantitative analysis of capillary density in peri-infarct area. Capillary density in the AM-MNC group was significantly higher than that in the MNC and AM groups. Values are means ± SE. *$P < 0.05$ vs. control; †$P < 0.05$ vs. MNC; ‡$P < 0.05$ vs. AM.

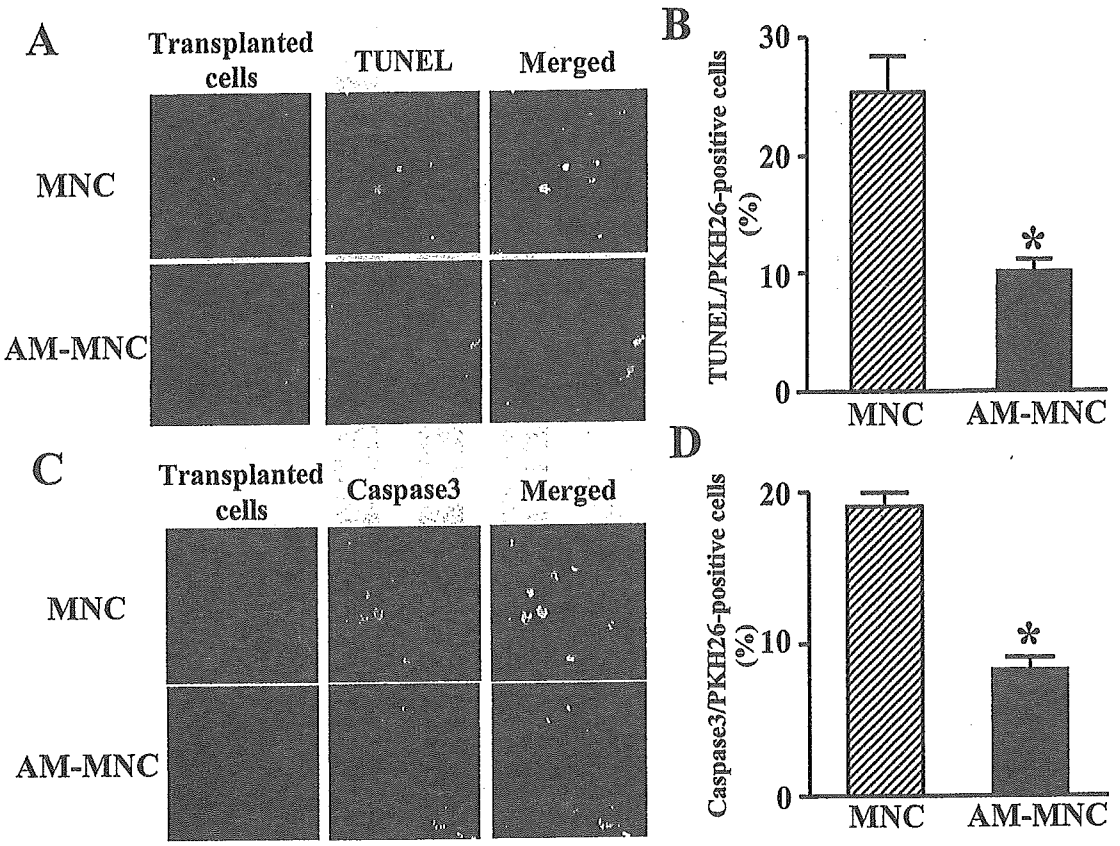

Fig. 4. Detection of transplanted cell apoptosis. *A*: representative photographs of terminal deoxynucleotidyl transferase-mediated dUTP nick end labeling (TUNEL) staining. Red fluorescence (PKH26) marks transplanted MNC; green fluorescence indicates TUNEL-positive cells. TUNEL-positive cells were frequently observed in the MNC group, whereas they were hardly detected in the AM-MNC group. Magnification, ×400. *B*: semiquantitative analysis of TUNEL-positive cells in the PKH26-positive (transplanted) cells. *C*: representative photographs of caspase-3 staining. Red fluorescence (PKH26) marks transplanted MNC; green fluorescence indicates caspase-3-positive cells. *D*: semiquantitative analysis of caspase-3-positive cells in the PKH26-positive cells. Values are means ± SE. *$P < 0.05$ vs. control.

were more frequently observed in the AM-MNC group than in the MNC group (6.4 ± 0.4 to 3.1 ± 0.2%, $P < 0.05$). Moreover, some of the transplanted cells were positive for UEA-1 lectin in the AM-MNC group (Fig. 5*A*), suggesting differentiation of MNC into vascular endothelial cells. Semiquantitative analysis demonstrated that the number of DAPI/PKH26 double-positive cells (viable transplanted cells) was significantly higher in the AM-MNC group than in the MNC group (Fig. 5*B*). Moreover, the ratio of lectin-positive cells to DAPI/PKH26 double-positive cells was significantly higher in the AM-MNC group than in the MNC group. The ratio of DAPI/PKH26 double-positive cells to lectin-positive cells was small, but significantly higher in the AM-MNC group than in the MNC group (23.9 ± 0.9 to 17.2 ± 0.6%, $P < 0.01$). Transplanted MNC were negative for troponin T or α-smooth muscle actin-positive cells. Some of the transplanted MNC were positive for ED1, a marker of macrophage (data not shown).

DISCUSSION

In the present study, we demonstrated that *1*) infusion of AM enhanced the angiogenic potency of MNC in a rat model of acute myocardial infarction, resulting in decreased infarct size and improved cardiac function. We also demonstrated that *2*) AM induced angiogenesis and inhibited apoptosis of the transplanted MNC. Thus a combination of AM and MNC may have beneficial effects in rats with myocardial infarction, partly through the angiogenic potency of AM itself and through its antiapoptotic effect on MNC.

Bone marrow-derived MNC include a variety of stem and progenitor cells (1, 15, 19), some of which can differentiate into endothelial cells and secrete numerous cytokines and chemokines (6, 9, 10). Earlier studies (6, 9, 10, 23, 25) have shown that autologous bone marrow transplantation induces angiogenesis and improves LV function in animals and humans. However, some patients are refractory to this cell therapy. Thus an approach to augment the angiogenic potency of MNC transplantation is required.

The present study showed that MNC transplantation or AM infusion alone reduced infarct size. A combination of AM infusion and MNC transplantation resulted in further decreases in infarct size and LV chamber size. MNC transplantation or AM administration modestly improved LV function. On the other hand, a combination of MNC and AM significantly improved cardiac performance compared with MNC or AM alone, as indicated by increases in cardiac output, fractional shortening, and LV maximum dP/dt. Earlier studies (6, 9, 10) have reported that MNC transplantation induces therapeutic angiogenesis and preserves LV function through inhibition of cardiomyocyte apoptosis in animal models of myocardial infarction. We have shown that AM infusion during the acute phase of ischemia-reperfusion inhibits apoptosis of cardiomyocytes and produces hemodynamic improvement in an animal

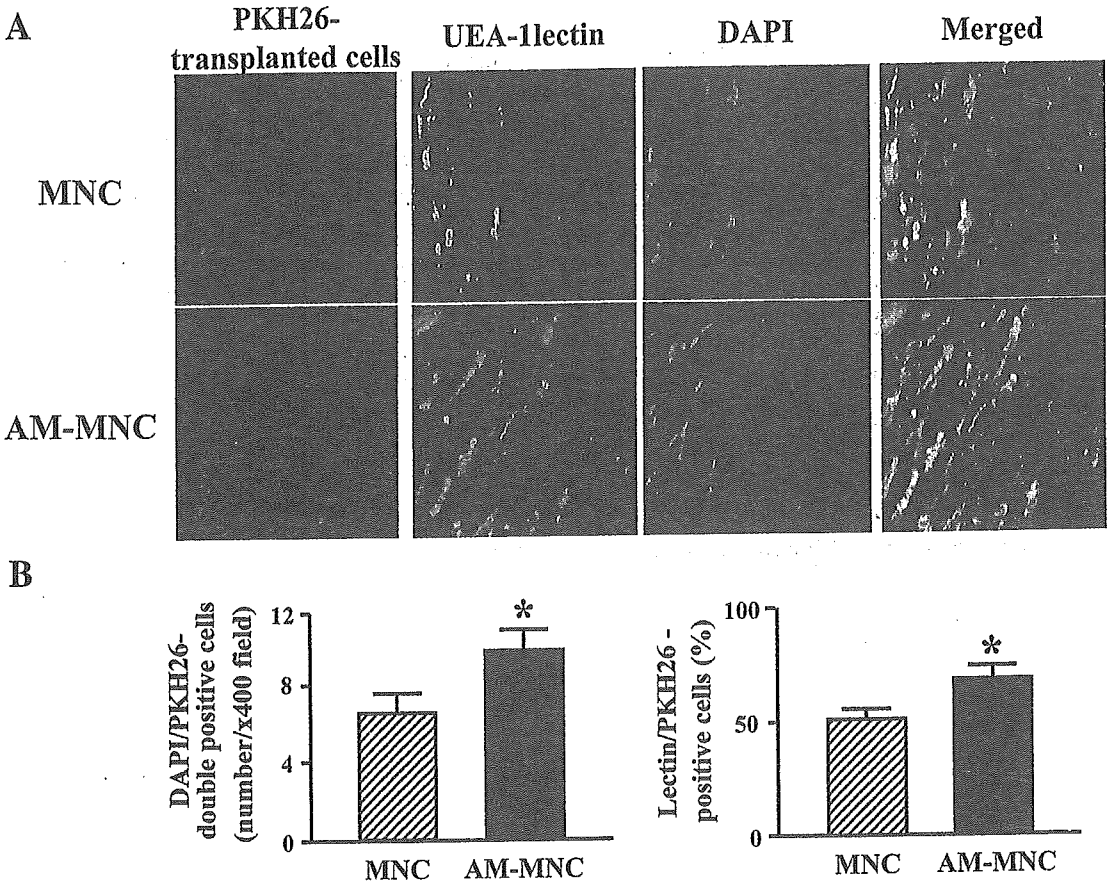

Fig. 5. *A*: representative examples of MNC differentiation into endothelial lineage. Red fluorescence (PKH26) marks transplanted cells; green fluorescence indicates ulex europaeus (UEA)-1 lectin, a marker for vascular endothelial cells. Most of the transplanted cells differentiated into endothelial cells in the AM-MNC group. Magnification, ×400. *B*: quantitative analysis of living transplanted cells and endothelial differentiation. The number of living cells after transplantation was significantly higher in the AM-MNC group than in the MNC group. The ratio of lectin-positive cells to living transplanted cells was significantly higher in the AM-MNC group than in the MNC group. Values are means ± SE. $^*P < 0.05$ vs. control. DAPI, 4′,6′-diamidino-2-phenylindole.

study (18). These findings suggest that the reduction of infarct size induced by this combination therapy may be attributable to additive cardioprotective effects of MNC and AM.

The present study showed that AM infusion significantly increased capillary density in ischemic myocardium. Furthermore, AM infusion plus MNC transplantation demonstrated a further increase in capillary density compared with AM or MNC alone. Contribution of transplanted MNC to neovascularization (the ratio of DAPI/PKH26 double-positive cells to lectin-positive cells) was significantly greater in the AM-MNC group than in the MNC group. A recent study (14) has reported that AM promotes proliferation and migration of human umbilical vein endothelial cells and enhances angiogenesis in a murine gel plug assay through the PI3-kinase/Akt pathway. We have also shown that intramuscular administration of AM DNA induces therapeutic angiogenesis in a rabbit model of chronic hindlimb ischemia via activation of Akt (24). These findings suggest that the beneficial effects of combination therapy using AM and MNC may be attributable, in part, to the angiogenic properties of AM itself. Thus it is possible that AM infusion and MNC transplantation induce additive effects on myocardial damage after myocardial infarction. However, it still remains unknown whether AM infusion plus MNC transplantation induces synergetic effects.

An earlier study has demonstrated that ischemia and mechanical stress induce apoptosis of transplanted cells in the early stage after MNC transplantation (9). These results raise the possibility that the angiogenic potency of MNC transplantation is attenuated by MNC apoptosis. Kim et al. (7) have demonstrated that AM inhibits apoptosis of endothelial cells through the PI3-kinase/Akt pathway in vitro. Activation of the PI3-kinase/Akt pathway has been shown to inhibit apoptosis of endothelial progenitor cells and enhance neovascularization (11). In the present study, AM infusion significantly inhibited MNC apoptosis in ischemic tissue. In vitro, we showed that the antiapoptotic effect of AM on MNC was mediated by activation of the PI3-kinase/Akt pathway. Thus AM may enhance the therapeutic potency of MNC transplantation through a direct action of AM on MNC survival. Moreover, immunohistological examination demonstrated that infusion of AM increased the number of lectin-positive (endothelial) cells in transplanted MNC. These findings raise the possibility that AM may enhance differentiation of MNC into the endothelial lineage. Thus AM may directly act on transplanted MNC, which may result in synergetic effects on the ischemic myocardium.

This study includes some study limitations. Although the labeling efficacy of PKH26 has been shown to persist for >8 wk without cell toxicity (3, 4), the used vital marker PKH26

may have some cell toxic effects and cell or membrane fusion can lead to labeling of neighboring cells in the target tissue. Second, the present study demonstrated that AM prolongs MNC survival through the PI3-kinase/Akt pathway and enhances neovascularization in a peri-infarcted area. However, further studies are necessary to examine the effect of AM on MNC differentiation into endothelial cells.

Autologous cell transplantation may be an alternative treatment for ischemic heart disease in the clinical setting. Because their use does not require immunosuppression, the clinical use of MNC for cellular cardiomyoplasty appears to be most advantageous. Administration of AM peptide is simple and relatively noninvasive. We and others (12, 16, 17) have reported the safety of AM infusion in humans. Thus combination therapy using AM infusion and MNC transplantation may be a new therapeutic strategy for the treatment of ischemic heart disease.

In conclusion, infusion of AM enhanced the angiogenic potency of MNC transplantation and improved cardiac function in rats with myocardial infarction. This beneficial effect may be mediated partly by the angiogenic property of AM itself and by its antiapoptotic effect on MNC. Thus combination therapy using AM infusion and MNC transplantation may be a new therapeutic strategy for the treatment of ischemic heart disease.

GRANTS

This work was supported by Ministry of Education, Culture, Sports, Science and Technology Grant-in-Aid for Scientific Research 13470154; Health and Labor Sciences Research Grants nano 001 and genome 005; Ministry of Health, Labor and Welfare Research Grant for Cardiovascular Disease H13C-1 and 16C-6; and grants from New Energy and Industrial Technology Development Organization and the Promotion of Fundamental Studies in Health Science of the Organization for Pharmaceutical Safety and Research of Japan.

REFERENCES

1. **Asahara T, Murohara T, Sullivan A, Silver M, van der Zee R, Li T, Witzenbichler B, Schatteman G, and Isner JM.** Isolation of putative progenitor endothelial cells for angiogenesis. *Science* 275: 964–967, 1997.
2. **Chien YW, Barbee RW, MacPhee AA, Frohlich ED, and Trippodo NC.** Increased ANF secretion after volume expansion is preserved in rats with heart failure. *Am J Physiol Regul Integr Comp Physiol* 254: R185–R191, 1988.
3. **Fox D, Kouris GJ, Blumofe KA, Heilizer TJ, Husak V, and Greisler HP.** Optimizing fluorescent labeling of endothelial cells for tracking during long-term studies of autologous transplantation. *J Surg Res* 86: 9–16, 1999.
4. **Gulbins H, Pritisanac A, Anderson I, Uhlig A, Goldemund A, Daebritz S, Meiser B, and Reichart B.** Myoblasts for survive 16 weeks after intracardiac transfer and start differentiation. *Thorac Cardiovasc Surg* 51: 295–300, 2003.
5. **Hennekens CH.** Increasing burden of cardiovascular disease: current knowledge and future directions for research on risk factors. *Circulation* 97: 1095–1102, 1998.
6. **Kamihata H, Matsubara H, Nishiue T, Fujiyama S, Tsutsumi Y, Ozono R, Masaki H, Mori Y, Iba O, Tateishi E, Kosaki A, Shintani S, Murohara T, Imaizumi T, and Iwasaka T.** Implantation of bone marrow mononuclear cells into ischemic myocardium enhances collateral perfusion and regional function via side supply of angioblasts, angiogenic ligands, and cytokines. *Circulation* 104: 1046–1052, 2001.
7. **Kim W, Moon SO, Sung MJ, Kim SH, Lee S, So JN, and Park SK.** Angiogenic role of adrenomedullin through activation of Akt, mitogen-activated protein kinase, and focal adhesion kinase in endothelial cells. *FASEB J* 17: 1937–1939, 2003.
8. **Kitamura K, Kangawa K, Kawamoto M, Ichiki Y, Nakamura S, Matsuo H, and Eto T.** Adrenomedullin: a novel hypotensive peptide isolated from human pheochromocytoma. *Biochem Biophys Res Commun* 192: 553–560, 1993.
9. **Kobayashi T, Hamano K, Li TS, Katoh T, Kobayashi S, Matsuzaki M, and Esato K.** Enhancement of angiogenesis by the implantation of self bone marrow cells in a rat ischemic heart model. *J Surg Res* 89: 189–195, 2000.
10. **Kocher AA, Schuster MD, Szabolcs MJ, Takuma S, Burkhoff D, Wang J, Homma S, Edwards NM, and Itescu S.** Neovascularization of ischemic myocardium by human bone-marrow-derived angioblasts prevents cardiomyocyte apoptosis, reduces remodeling and improves cardiac function. *Nat Med* 7: 430–436, 2001.
11. **Llevadot J, Murasawa S, Kureishi Y, Uchida S, Masuda H, Kawamoto A, Walsh K, Isner JM, and Asahara T.** HMG-CoA reductase inhibitor mobilizes bone marrow-derived endothelial progenitor cells. *J Clin Invest* 108: 399–405, 2001.
12. **McGregor DO, Troughton RW, Frampton C, Lynn KL, Yandle T, Richards AM, and Nicholls MG.** Hypotensive and natriuretic actions of adrenomedullin in subjects with chronic renal impairment. *Hypertension* 37: 1279–1284, 2001.
13. **Messina LM, Podrazik RM, Whitehill TA, Ekhterae D, Brothers TE, Wilson JM, Burkel WE, and Stanley JC.** Adhesion and incorporation of lacZ-transduced endothelial cells into the intact capillary wall in the rat. *Proc Natl Acad Sci USA* 89: 12018–12022, 1992.
14. **Miyashita K, Itoh H, Sawada N, Fukunaga Y, Sone M, Yamahara K, Yurugi-Kobayashi T, Park K, and Nakao K.** Adrenomedullin provokes endothelial Akt activation and promotes vascular regeneration both in vitro and in vivo. *FEBS Lett* 544: 86–92, 2003.
15. **Murohara T, Ikeda H, Duan J, Shintani S, Sasaki K, Eguchi H, Onitsuka I, Matsui K, and Imaizumi T.** Transplanted cord blood-derived endothelial precursor cells augment postnatal neovascularization. *J Clin Invest* 105: 1527–1536, 2000.
16. **Nagaya N, Kyotani S, Uematsu M, Ueno K, Oya H, Nakanishi N, Shirai M, Mori H, Miyatake K, and Kangawa K.** Effects of adrenomedullin inhalation on hemodynamics and exercise capacity in patients with idiopathic pulmonary hypertension. *Circulation* 109: 351–356, 2004.
17. **Nagaya N, Satoh T, Nishikimi T, Uematsu M, Furuichi S, Sakamaki F, Oya H, Kyotani S, Nakanishi N, Goto Y, Masuda Y, Miyatake K, and Kangawa K.** Hemodynamic, renal, and hormonal effects of adrenomedullin infusion in patients with congestive heart failure. *Circulation* 101: 498–503, 2000.
18. **Okumura H, Nagaya N, Itoh T, Okano I, Hino J, Mori K, Tsukamoto Y, Ishibashi-Ueda H, Miwa S, Tambara K, Toyokuni S, Yutani C, and Kangawa K.** Adrenomedullin infusion attenuates myocardial ischemia/reperfusion injury through the phosphatidylinositol 3-kinase/Akt-dependent pathway. *Circulation* 109: 242–248, 2004.
19. **Rafii S and Lyden D.** Therapeutic stem and progenitor cell transplantation for organ vascularization and regeneration. *Nat Med* 9: 702–712, 2003.
20. **Sata M, Kakoki M, Nagata D, Nishimatsu H, Suzuki E, Aoyagi T, Sugiura S, Kojima H, Nagano T, Kangawa K, Matsuo H, Omata M, Nagai R, and Hirata Y.** Adrenomedullin and nitric oxide inhibit human endothelial cell apoptosis via a cyclic GMP-independent mechanism. *Hypertension* 36: 83–88, 2000.
21. **Schiller NB, Shah PM, Crawford M, DeMaria A, Devereux R, Feigenbaum H, Gutgesell H, Reichek N, Sahn D, Schnittger I, Silverman NH, and Tajik AJ.** Recommendations for quantitation of the left ventricle by two-dimensional echocardiography. American Society of Echocardiography Committee on Standards, Subcommittee on Quantitation of Two-Dimensional Echocardiograms. *J Am Soc Echocardiogr* 2: 358–367, 1989.
22. **Shiojima I and Walsh K.** Role of Akt signaling in vascular homeostasis and angiogenesis. *Circ Res* 90: 1243–1250, 2002.
23. **Strauer BE, Brehm M, Zeus T, Kostering M, Hernandez A, Sorg RV, Kogler G, and Wernet P.** Repair of infarcted myocardium by autologous intracoronary mononuclear bone marrow cell transplantation in humans. *Circulation* 106: 1913–1918, 2002.
24. **Tokunaga N, Nagaya N, Shirai M, Tanaka E, Ishibashi-Ueda H, Harada-Shiba M, Kanda M, Ito T, Shimizu W, Tabata Y, Uematsu M, Nishigami K, Sano S, Kangawa K, and Mori H.** Adrenomedullin gene transfer induces therapeutic angiogenesis in a rabbit model of chronic hind limb ischemia: benefits of a novel nonviral vector, gelatin. *Circulation* 109: 526–531, 2004.
25. **Tse HF, Kwong YL, Chan JK, Lo G, Ho CL, and Lau CP.** Angiogenesis in ischaemic myocardium by intramyocardial autologous bone marrow mononuclear cell implantation. *Lancet* 361: 47–49, 2003.

Honorable Mention Poster Award

High-speed K-edge angiography achieved with tantalum K-series characteristic x rays

Eiichi Sato*[a], Etsuro Tanaka[b], Hidezo Mori[c], Toshiaki Kawai[d], Takashi Inoue[c], Akira Ogawa[c], Shigehiro Sato[f], Kazuyoshi Takayama[g] and Hideaki Ido[h]

[a] Department of Physics, Iwate Medical University, 3-16-1 Honchodori, Morioka 020-0015, Japan,
[b] Department of Nutritional Science, Faculty of Applied Bio-science, Tokyo University of Agriculture, 1-1-1 Sakuragaoka, Setagaya-ku 156-8502, Japan
[c] Department of Cardiac Physiology, National Cardiovascular Center Research Institute, 5-7-1 Fujishirodai, Suita, Osaka 565-8565, Japan
[d] Electron Tube Division #2, Hamamatsu Photonics K. K., 314-5 Shimokanzo, Toyooka Village, Iwata-gun 438-0193, Japan
[e] Department of Neurosurgery, School of Medicine, Iwate Medical University, 19-1 Uchimaru, Morioka 020-8505, Japan
[f] Department of Microbiology, School of Medicine, Iwate Medical University, 19-1 Uchimaru, Morioka 020-8505, Japan
[g] Shock Wave Research Center, Institute of Fluid Science, Tohoku University, 2-1-1 Katahira, Sendai 980-8577, Japan
[h] Department of Applied Physics and Informatics, Faculty of Engineering, Tohoku Gakuin University, 1-13-1 Chuo, Tagajo 985-8537, Japan

ABSTRACT

The tantalum plasma flash x-ray generator is useful in order to perform high-speed K-edge angiography using cone beams because Kα rays from the tantalum target are absorbed effectively by gadolinium-based contrast media. In the flash x-ray generator, a 150 nF condenser is charged up to 80 kV by a power supply, and flash x rays are produced by the discharging. The x-ray tube is a demountable diode, and the turbomolecular pump evacuates air from the tube with a pressure of approximately 1 mPa. Since the electric circuit of the high-voltage pulse generator employs a cable transmission line, the high-voltage pulse generator produces twice the potential of the condenser charging voltage. When the charging voltage was increased, the K-series characteristic x-ray intensities of tantalum increased. The K lines were clean and intense, and hardly any bremsstrahlung rays were detected. The x-ray pulse widths were approximately 100 ns, and the time-integrated x-ray intensity had a value of approximately 300 μGy at 1.0 m from the x-ray source with a charging voltage of 80 kV. Angiography was performed using a film-less computed radiography (CR) system and gadolinium-based contrast media. In angiography of non-living animals, we observed fine blood vessels of approximately 100 μm with high contrasts.

Keywords: angiography, gadolinium-based contrast media, characteristic x rays, quasi-monochromatic x rays, tantalum Kα photons

1. INTRODUCTION

The successful uses of monochromatic parallel beams from synchrotron orbital radiation in recent years have greatly increased the demand for phase-contrast radiography[1-3] and enhanced K-edge angiography.[4-6] In particular, the parallel beams with photon energies of approximately 35 keV have been employed to perform angiography, because the beams are absorbed effectively by iodine-based contrast media with a K-absorption edge of 33.2 keV. Without using a synchrotron, we have developed an x-ray generator utilizing a cerium-target tube, and have performed cone-beam K-edge angiography achieved with cerium Kα rays of 34.6 keV.[7] However, the x-ray intensity rate was limited because

Medical Imaging 2005: Physics of Medical Imaging, edited by Michael J. Flynn,
Proceedings of SPIE Vol. 5745 (SPIE, Bellingham, WA, 2005)
1605-7422/05/$15 · doi: 10.1117/12.601547

the thermal contact between the target and the anode was not good.
Although various flash x-ray generators have been developed,[8] we have developed flash x-ray generators[9-13] with photon energies of less than 150 keV in order to primarily perform high-speed biomedical radiography. Subsequently, we have developed plasma flash x-ray generators[14-16] to perform a preliminary experiment for producing hard x-ray lasers from weakly ionized linear plasma, and have succeeded in producing intense and clean K-series characteristic x rays using copper and nickel targets. In addition, we have confirmed the weak hard x-ray resonation verified from irradiation of weakly higher harmonic x rays. However, it is difficult to produce high-photon-energy characteristic x rays because the plasma transmits high-photon-energy bremsstrahlung x rays. Therefore, we developed a quasi-monochromatic flash x-ray generator[17,18] with a disk-cathode tube to produce high-energy characteristic x rays utilizing the angle dependence of bremsstrahlung x-ray distribution, because the bremsstrahlung rays are not emitted in the apposite direction to that of electron acceleration. Using this generator, we have succeeded in producing clean characteristic x rays from molybdenum, silver and cerium targets.
Gadolinium-based contrast media with a K-edge of 50.2 keV have been employed to perform angiography in MRI, and the gadolinium density has been increasing. In view of this situation, ytterbium Kα rays (52.0 keV) are useful for enhanced K-edge angiography, because the Kα rays are absorbed effectively by gadolinium media. As compared with angiography using iodine media, the absorbed dose can be decreased considerably utilizing angiography achieved with gadolinium media. However, because ytterbium is a lanthanide series element and has a high reactivity, Kα rays of tantalum and tungsten are also useful to perform angiography.
In this article, we describe an intense quasi-monochromatic plasma flash x-ray generator with a tantalum target tube, and used it to perform a preliminary study on angiography achieved with tantalum K-series characteristic x rays.

2. PRINCIPLE OF K-EDGE ANGIOGRAPHY

Figure 1 shows the mass attenuation coefficients of gadolinium at the selected energies; the coefficient curve is discontinuous at the gadolinium K-edge. The average photon energy of the tantalum Kα lines is shown above the gadolinium K-edge. The average photon energy of tantalum Kα lines is 57.1 keV, and gadolinium contrast media with a K-absorption edge of 50.2 keV absorb the lines easily. Therefore, blood vessels were observed with high contrasts.

3. GENERATOR

3.1 High-voltage circuit

Figure 2 shows a block diagram of a high-intensity plasma flash x-ray generator. The generator consists of the following essential components: a high-voltage power supply, a high-voltage condenser with a capacity of approximately 150 nF, an air gap switch, a turbomolecular pump, a thyratron pulse generator as a trigger device, and a flash x-ray tube. In this generator, a coaxial cable transmission line is employed in order to increase maximum tube voltage using high-voltage reflection (Fig. 3). The high-voltage main condenser is charged up to 80 kV by the power supply, and electric charges in the condenser are discharged to the tube through the four cables after closing the gap switch with the trigger device.

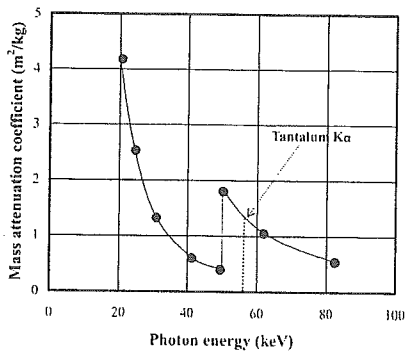

Figure 1: Relation between mass attenuation coefficient of gadolinium and average photon energy of tantalum Kα lines.

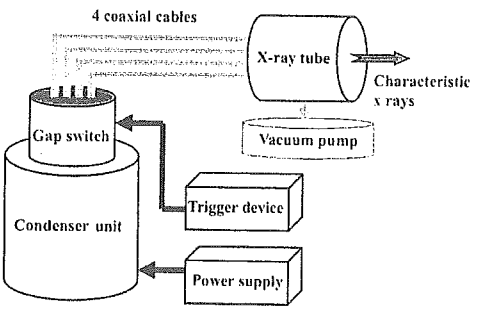

Figure 2: Block diagram of intense quasi-monochromatic flash x-ray generator.

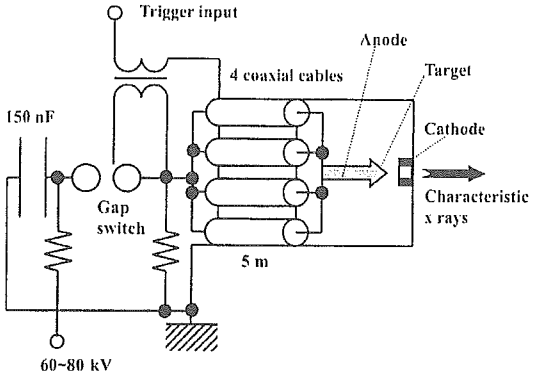

Figure 3: High-voltage circuit of flash x-ray generator.

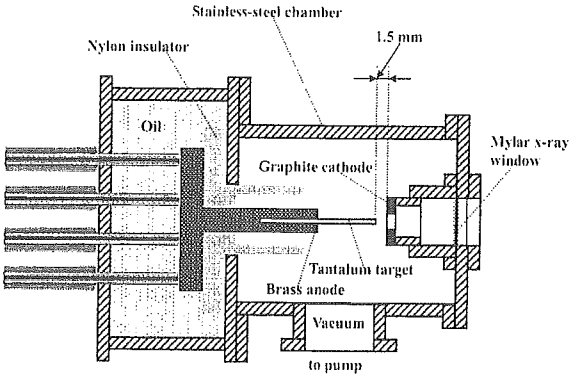

Figure 4: Schematic drawing of flash x-ray tube.

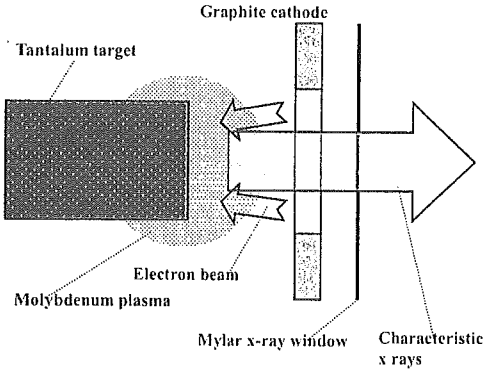

Figure 5: Irradiation of characteristic x rays.

3.2 X-ray tube

The x-ray tube is a demountable cold-cathode diode that is connected to the turbomolecular pump with a pressure of approximately 1 mPa (Fig. 4). This tube consists of the following major parts: a ring-shaped graphite cathode with an bore diameter of 4.5 mm, a stainless-steel vacuum chamber, a nylon insulator, a polyethylene terephthalate (Mylar) x-ray window 0.25 mm in thickness, and a rod-shaped tantalum target 3.0 mm in diameter. The distance between the target and cathode electrodes can be regulated from the outside of the tube, and is set to 1.5 mm. As electron beams from the cathode electrode are roughly converged to the target by the electric field in the tube, evaporation leads to the formation of weakly ionized plasma, consisting of tantalum ions and electrons, around the target. Because bremsstrahlung rays are not emitted in the opposite direction to that of electron acceleration (Fig. 5), tantalum K-series characteristic x rays can be produced without using a filter.

4. CHARACTERISTICS

4.1 Tube voltage and current

In this generator, it was difficult to measure the tube voltage and current since the tube voltages were high, and there was no space to set a current transformer for measuring the tube current. Currently, the voltage and current roughly display damped oscillations. When the charging voltage was increased, both the maximum tube voltage and current increased. At a charging voltage of 80 kV, the estimated maximum values of the tube voltage and current were approximately 160 kV (2 times the charging voltage) and 40 kA, respectively.

4.2 X-ray output

X-ray output pulse was detected using a combination of a plastic scintillator and a photomultiplier (Fig. 6). The x-ray pulse height substantially increased with corresponding increases in the charging voltage. The x-ray pulse widths were approximately 100 ns, and the time-integrated x-ray intensity measured by a thermoluminescence dosimeter (Kyokko TLD Reader 1500 having MSO-S elements without energy compensation) had a value of approximately 300 μGy at 1.0 m from the x-ray source with a charging voltage of 80 kV.

4.3 X-ray source

In order to observe the characteristic x-ray source, we employed a 100-μm-diameter pinhole camera and an x-ray film (Polaroid XR-7) (Fig. 7). When the charging voltage was increased, the plasma x-ray source grew, and both spot dimension and intensity increased. Because the x-ray intensity is the highest at the center of the spot, both the dimension and intensity decreased according to decreases in the pinhole diameter.

4.4 X-ray spectra

X-ray spectra were measured using a transmission-type spectrometer with a lithium fluoride curved crystal 0.5 mm in thickness. The x-ray intensities of the spectra were detected by an imaging plate of a computed radiography (CR) system[19] (Konica Regius 150) with a wide dynamic range, and relative x-ray intensity was calculated from Dicom original digital data corresponding to x-ray intensity; the data was scanned by Dicom viewer in the film-less CR system. Subsequently, the relative x-ray intensity as a function of the data was calibrated using a conventional x-ray generator, and we confirmed that the intensity was proportional to the exposure time. Figure 8 shows measured spectra from the tantalum target. We observed clean K-series lines, while bremsstrahlung rays were hardly detected. The characteristic x-ray intensity substantially increased with increases in the charging voltage.

5. ANGIOGRAPHY

The flash angiography was performed by a computed radiography (CR) system (Konica Regius 150)[19] at 1.2 m from the x-ray source, and the charging voltage was 80 kV.

Firstly, rough measurements of spatial resolution were made using wires. Figure 9 shows radiograms of tungsten wires coiled around a rod made of polymethyl methacrylate. Although the image contrast decreased somewhat with decreases in the wire diameter, due to blurring of the image caused by the sampling pitch of 87.5 μm, a 50 μm-diameter wire could be observed. Because the tungsten wires transmitted the characteristic x rays easily, low contrast radiograms were obtained.

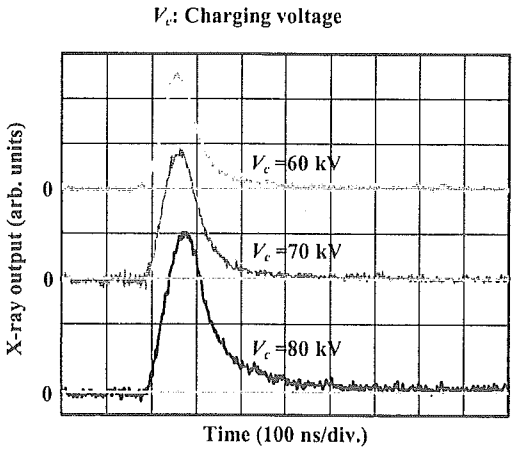

Figure 6: X-ray outputs at indicated conditions.

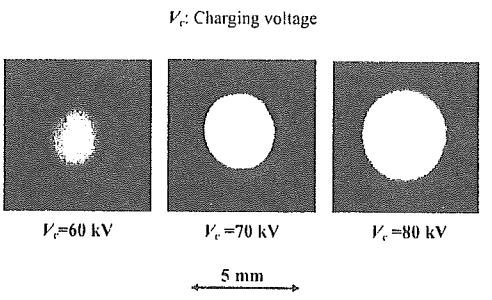

Figure 7: Images of characteristic x-ray source with changes in charging voltage.

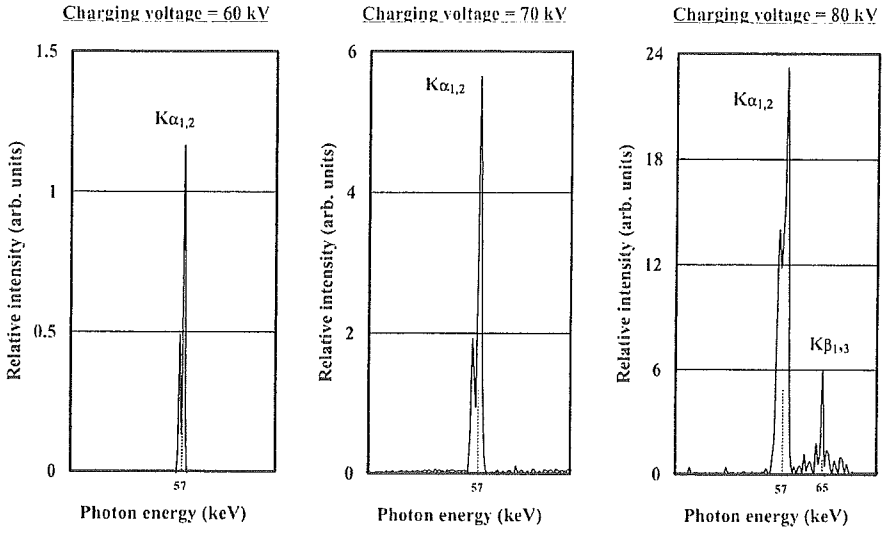

Figure 8: X-ray spectra from tantalum target.

The image of water (gadolinium oxide suspension of 20%) falling into a polypropylene beaker from a plastic test tube is shown in Fig. 10. The diameter of gadolinium oxide powder ranges from 1 to 10 μm. Because the x-ray duration was about 100 ns, the stop-motion image of water could be obtained.
Figure 11 shows an angiogram of a silicone rubber tube in a polymethyl methacrylate (PMMA) case using a contrast medium which contains 32.3% gadodiamidehydrate, and a low contrast tube with a bore diameter of 1.0 mm is observed. In cases where a gadolinium oxide suspension of 50% is employed, high-contrast angiography of the tubes (1.0 mm and 0.5 mm in bore diameter) could be performed (Fig. 12). Figure 13 shows an angiogram of a rabbit head using gadolinium oxide powder, and fine blood vessels of approximately 100 μm were visible.

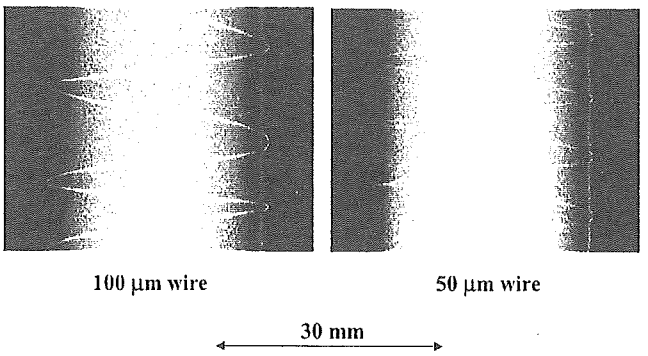

Figure 9: Radiograms of tungsten wires coiled around rod made of polymethyl methacrylate.

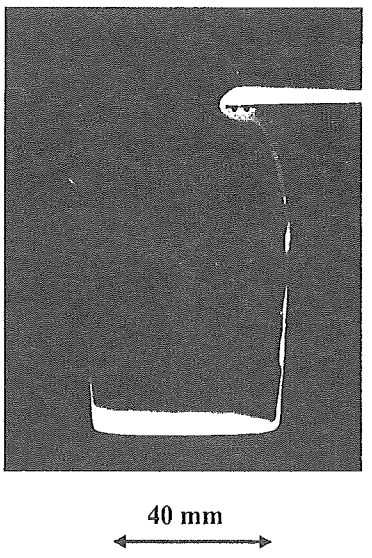

Figure 10: Radiogram of water falling into polypropylene beaker from plastic test tube.

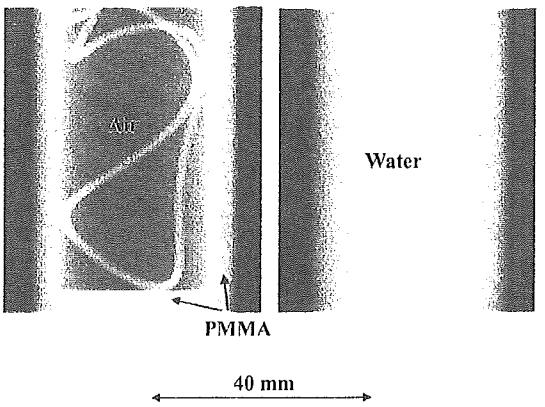

Figure 11: Angiograms of silicon tube using contrast medium of 32.3% gadodiamidehydrate.

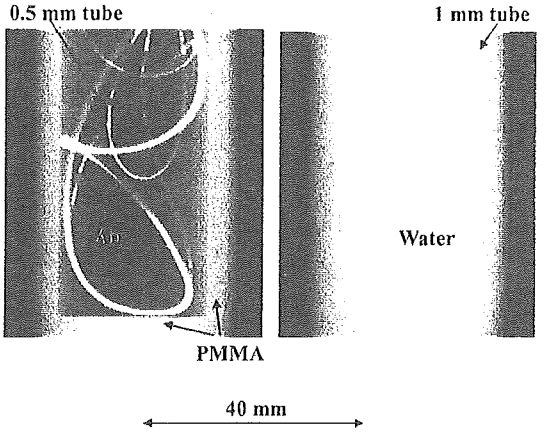

Figure 12: Angiography of silicon tube using gadolinium oxide suspension of 50%.

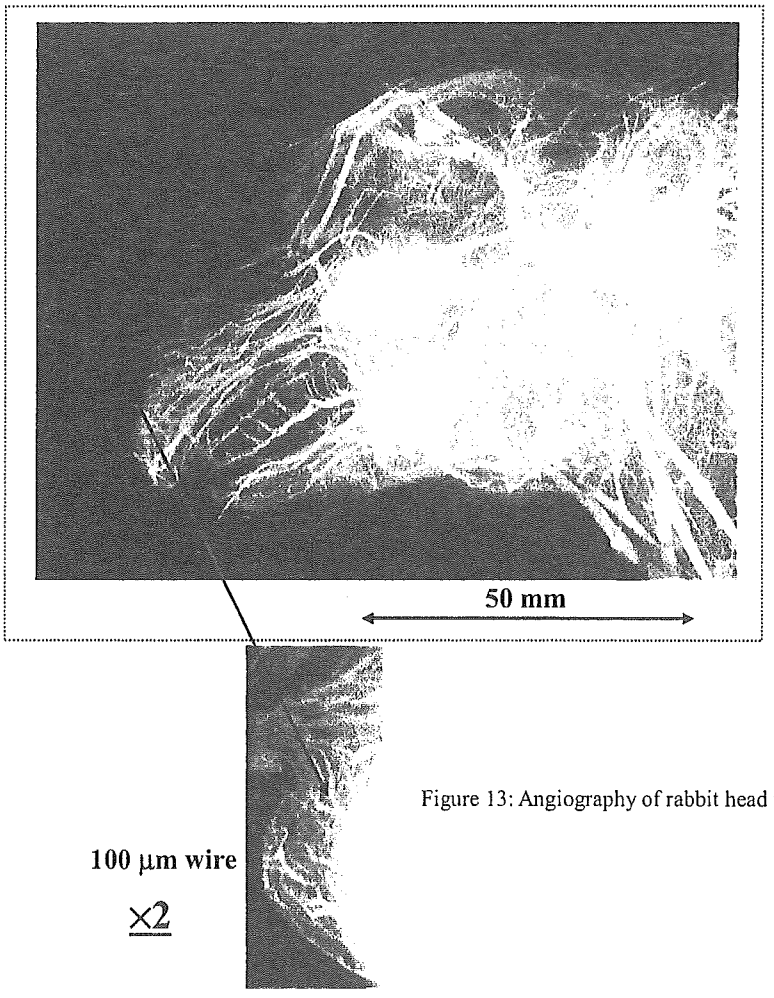

Figure 13: Angiography of rabbit head using gadolinium oxide powder.

6. DISCUSSION AND CONCLUSIONS

In summary, we succeeded in producing K-series characteristic x rays of tantalum and in performing K-edge angiography using gadolinium contrast media with a K-edge of 50.2 keV, and this K-edge angiography could be a useful technique to decrease the dose absorbed by patients. Although we employed tantalum Kα (57.1 keV) and Kβ (approximately 65 keV) rays, Kβ rays should be absorbed using an ytterbium oxide filter with an ytterbium K edge of 61.3 keV in order to increase the image contrast of blood vessels.

To perform K-edge angiography using gadolinium media, although an ytterbium target with a Kα energy of 52.0 keV is useful, the ytterbium has a high reactivity. If we assume that the ytterbium is employed, an alloy target should be developed. In this research, we obtained sufficient x-ray intensity per pulse for angiography, and the intensity can be increased by increasing the electrostatic energies in the high-voltage condenser. At a condenser capacity of 150 nF, the generator produced instantaneous number of K photons was approximately 1×10^9 photons/cm^2 per pulse at 1.0 m from the source.

In the flash x-ray tube, bremsstrahlung x rays with energies higher than the K-edge are absorbed effectively by the weakly ionized plasma and are converted into fluorescent (characteristic) x rays. In conjunction with this property, because the bremsstrahlung x rays are not emitted in the opposite direction to that of electron acceleration, clean characteristic x rays are produced. Using this flash x-ray generator, with which the photon energy of characteristic x rays can be selected, quasi-monochromatic imaging such as enhanced K-edge angiography using iodine contrast media and mammography can be performed.

ACKNOWLEDGMENT

This work was supported by Grants-in-Aid for Scientific Research (13470154, 13877114, 16591181, and 16591222) and Advanced Medical Scientific Research from MECSST, Health and Labor Sciences Research Grants(RAMT-nano-001, RHGTEFB-genome-005 and RHGTEFB-saisei-003), Grants from Keiryo Research Foundation, The Promotion and Mutual Aid Corporation for Private Schools of Japan, Japan Science and Technology Agency (JST), and New Energy and Industrial Technology Development Organization (NEDO, Industrial Technology Research Grant Program in '03).

REFERENCES

1. T. J. Davis, D. Gao, T. E. Gureyev, A. W. Stevenson and S. W. Wilkins, "Phase-contrast imagimg of weakly absorbing materials using hard x-rays," *Nature*, **373**, 595-597, 1995.

2. A. Momose, T. Takeda, Y. Itai and K. Hirano, "Phase-contrast x-ray computed tomography for observing biological soft tissues," *Nature Medicine*, **2**, 473-475, 1996.

3. M. Ando, A. Maksimenko, H. Sugiyama, W. Pattanasiriwisawa, K. Hyodo and C. Uyama, "A simple x-ray dark- and bright- field imaging using achromatic Laue optics," *Jpn. J. Appl. Phys.*, **41**, L1016-L1018, 2002.

4. A. C. Thompson, H. D. Zeman, G. S. Brown, J. Morrison, P. Reiser, V. Padmanabahn, L. Ong, S. Green, J. Giacomini, H. Gordon and E. Rubenstein, "First operation of the medical research facility at the NSLS for coronary angiography," *Rev. Sci. Instrum.*, **63**, 625-628, 1992.

5. H. Mori, K. Hyodo, E. Tanaka, M. U. Mohammed, A. Yamakawa, Y. Shinozaki, H. Nakazawa, Y. Tanaka, T. Sekka, Y. Iwata, S. Honda, K. Umetani, H. Ueki, T. Yokoyama, K. Tanioka, M. Kubota, H. Hosaka, N. Ishizawa and M. Ando, "Small-vessel radiography in situ with monochromatic synchrotoron radiation," *Radiology*, **201**, 173-177, 1996.

6. K. Hyodo, M. Ando, Y. Oku, S. Yamamoto, T. Takeda, Y. Itai, S. Ohtsuka, Y. Sugishita and J. Tada, "Development of a two-dimensional imaging system for clinical applications of intravenous coronary angiography using intense synchrotron radiation produced by a multipole wiggler," *J. Synchrotron Rad.*, **5**, 1123-1126, 1998.

7. E. Sato, E. Tanaka, H. Mori, T. Kawai, T. Ichimaru, S. Sato, K. Takayama and H. Ido, "Demonstration of enhanced K-edge angiography using a cerium target x-ray generator," *Med. Phys*, **31**, 3017-3021, 2004.

8. R. Germer, "X-ray flash techniques," *J. Phys. E: Sci. Instrum.*, **12**, 336-350, 1979.

9. E. Sato, S. Kimura, S. Kawasaki, H. Isobe, K. Takahashi, Y. Tamakawa and T. Yanagisawa, "Repetitive flash x-ray generator utilizing a simple diode with a new type of energy-selective function," *Rev. Sci. Instrum.*, **61**, 2343-2348, 1990.

10. A. Shikoda, E. Sato, M. Sagae, T. Oizumi, Y. Tamakawa and T. Yanagisawa, "Repetitive flash x-ray generator having a high-durability diode driven by a two-cable-type line pulser," *Rev. Sci. Instrum.*, **65**, 850-856, 1994.
11. E. Sato, K. Takahashi, M. Sagae, S. Kimura, T. Oizumi, Y. Hayasi, Y. Tamakawa and T. Yanagisawa, "Sub-kilohertz flash x-ray generator utilizing a glass-enclosed cold-cathode triode," *Med. & Biol. Eng. & Comput.*, **32**, 289-294, 1994.
12. K. Takahashi, E. Sato, M. Sagae, T. Oizumi, Y. Tamakawa and T. Yanagisawa, "Fundamental study on a long-duration flash x-ray generator with a surface-discharge triode," *Jpn. J. Appl. Phys.*, **33**, 4146-4151, 1994.
13. E. Sato, M. Sagae, K. Takahashi, A. Shikoda, T. Oizumi, Y. Hayasi, Y. Tamakawa and T. Yanagisawa, "10 kHz microsecond pulsed x-ray generator utilizing a hot-cathode triode with variable durations for biomedical radiography," *Med. & Biol. Eng. & Comput.*, **32**, 295-301, 1994.
14. E. Sato, Y. Hayasi, R. Germer, E. Tanaka, H. Mori, T. Kawai, H. Obara, T. Ichimaru, K. Takayama and H. Ido, "Irradiation of intense characteristic x-rays from weakly ionized linear molybdenum plasma," *Jpn. J. Med. Phys.*, **23**, 123-131, 2003.
15. E. Sato, Y. Hayasi, R. Germer, E. Tanaka, H. Mori, T. Kawai, T. Ichimaru, K. Takayama and H. Ido, "Quasi-monochromatic flash x-ray generator utilizing weakly ionized linear copper plasma," *Rev. Sci. Instrum.*, **74**, 5236-5240, 2003.
16. E. Sato, Y. Hayasi, R. Germer, E. Tanaka, H. Mori, T. Kawai, T. Ichimaru, S. Sato, K. Takayama and H. Ido, "Sharp characteristic x-ray irradiation from weakly ionized linear plasma," *J. Electron Spectrosc. Related Phenom.*, **137-140**, 713-720, 2004.
17. E. Sato, M. Sagae, E. Tanaka, Y. Hayasi, R. Germer, H. Mori, T. Kawai, T. Ichimaru, S. Sato, K. Takayama and H. Ido, "Quasi-monochromatic flash x-ray generator utilizing a disk-cathode molybdenum tube," *Jpn. J. Appl. Phys.*, **43**, 7324-7328, 2004.
18. E. Sato, E. Tanaka, H. Mori, T. Kawai, T. Ichimaru, S. Sato, K. Takayama and H. Ido, "Compact monochromatic flash x-ray generator utilizing a disk-cathode molybdenum tube," *Med. Phys.*, **32**, 49-54, 2005.
19. E. Sato, K. Sato and Y. Tamakawa, "Film-less computed radiography system for high-speed imaging," *Ann. Rep. Iwate Med. Univ. Sch. Lib. Arts and Sci.*, **35**, 13-23, 2000.

*dresato@iwate-med.ac.jp; phone +81-19-651-5111; fax +81-19-654-9282